

1 **A Coupled Ensemble Filtering and Probabilistic Collocation Approach for**
2 **Uncertainty Quantification of Hydrological Models**

3

4 Y.R. Fan^a, W.W. Huang^b, Y.P. Li^c, G.H. Huang^{c,d}, K. Huang^a

5

6 ^a Faculty of Engineering and Applied Science, University of Regina, Regina, Saskatchewan,
7 Canada S4S 0A2b

8 ^b Department of Civil Engineering, McMaster University, Hamilton, ON L8S 4L8, Canada

9 ^c MOE Key Laboratory of Regional Energy and Environmental Systems Optimization, North
10 China Electric Power University, Beijing 102206, China

11 ^d Institute for Energy, Environment and Sustainability Research, UR-NCEPU, University of
12 Regina, Regina, Saskatchewan, Canada S4S 0A2; Tel: +13065854095; Fax: +13065854855; E-
13 mail: huang@iseis.org

14

15 *Correspondence: Dr. G. H. Huang

16 Faculty of Engineering and Applied Sciences, University of Regina

17 Regina, Saskatchewan, S4S 0A2, Canada

18 Tel: (306) 585-4095

19 Fax: (306) 585-4855

20 E-mail: huangg@uregina.ca

21

22

23

24 **Abstract:**

25

26 In this study, a coupled ensemble filtering and probabilistic collocation (EFPC)
27 approach is proposed for uncertainty quantification of hydrologic models. This
28 approach combines the capabilities of the ensemble Kalman filter (EnKF) and the
29 probabilistic collocation method (PCM) to provide a better treatment of uncertainties
30 in hydrologic models. The EnKF method would be employed to approximate the
31 posterior probabilities of model parameters and improve the forecasting accuracy
32 based on the observed measurements; the PCM approach is proposed to construct a
33 model response surface in terms of the posterior probabilities of model parameters to
34 reveal uncertainty propagation from model parameters to model outputs. The
35 proposed method is applied to the Xiangxi River, located in the Three Gorges
36 Reservoir area of China. The results indicate that the proposed EFPC approach can
37 effectively quantify the uncertainty of hydrologic models. Even for a simple
38 conceptual hydrological model, the efficiency of EFPC approach is about 10 times
39 faster than traditional Monte Carlo method without obvious decrease in prediction
40 accuracy. Finally, the results can explicitly reveal the contributions of model
41 parameters to the total variance of model predictions during the simulation period.

42

43 **Keywords:** Uncertainty; Ensemble Kalman filter; Probabilistic collocation method;
44 Gaussian anamorphosis; Hydrologic model; Monte Carlo

45

46

47 **1. Introduction**

48 Hydrologic models are simplified, conceptual representations of a part of the
49 hydrologic cycle, which use relatively simple mathematical equations to
50 conceptualize and aggregate the complex, spatially distributed, and highly interrelated
51 water, energy, and vegetation processes in a watershed (Vrugt et al., 2005). Such
52 conceptualization and aggregation lead to extensive uncertainties involved in both
53 model parameters and structures, and consequently produce significant uncertainties
54 in hydrologic predictions. Uncertainty in hydrologic predictions can originate from
55 several major sources, including model structures, parameters, and measurement
56 errors in model inputs (Ajami et al., 2007; Liu et al., 2012). Therefore, effective
57 uncertainty quantification and reduction methods are required to produce reliable
58 hydrologic forecasts for many real-world water resources applications, such as
59 flooding control, drought management and reservoir operation (Fan et al., 2012; Kong
60 et al., 2015; Fan et al., 2015a).

61 Previously, a number of probabilistic estimation methods have been proposed for
62 quantifying uncertainty in hydrologic predictions. The probabilistic estimation
63 methods approximate the posterior probability distributions of the hydrological
64 parameters through the Bayesian theorem, conditioned on the streamflow
65 observations. The generalized likelihood uncertainty estimation (GLUE) (Beven and
66 Binley, 1992), Markov Chain Monte Carlo (Vrugt et al., 2009; Han et al., 2014),
67 Bayesian model averaging (BMA) (Diks and Vrugt., 2010), and approximate
68 Bayesian computation (Vrugt and Sadegh, 2013) methods are those extensively used
69 probabilistic estimation methods. For instance, Madadgar and Moradkhani (2014)
70 improved Bayesian Multi-modeling predictions through integration of copulas and
71 Bayesian model averaging methods. DeChant and Moradkhani (2014b) proposed a

72 full review of uncertainty quantification methods.

73 In a separate line of research, sequential data assimilation methods have been
74 developed to explicitly handle various uncertainties and optimally merging
75 observations into uncertain model predictions (Xie and Zhang, 2013; Zhang et al.,
76 2012a,b; Zhang and Yang, 2013, 2014; Chang and Sayemuzzaman, 2014; Assumaning
77 and Chang, 2014). In contrast to classical model calibration strategies, sequential data
78 assimilation approaches continuously update the states and parameters to improve
79 model forecasts when new measurements become available (Vrugt et al., 2005). The
80 prototype of sequential data assimilation techniques, the Kalman filter (KF) (Kalman,
81 1960) and the ensemble Kalman filter (EnKF) (Evensen, 1994), provide optimal
82 frameworks for linear dynamic models with Gaussian uncertainties. The EnKF
83 approach is one of the most frequently used data assimilation methods in hydrology
84 due to its attractive features of real-time adjustment and easy implementation (Reichle
85 et al., 2002). The EnKF method can provide a general framework for dynamic state,
86 parameter, and joint state-parameter estimation in hydrologic models. For example,
87 Moradkhani et al. (2005a) proposed a dual-state estimation approach based on EnKF
88 for sequential estimation for both parameters and state variables of a hydrologic
89 model. Weerts and El Serafy (2006) compared the capability of EnKF and particle
90 filter (PF) methods in reducing uncertainty in the rainfall-runoff update and internal
91 model state estimation for flooding forecasting purposes. Parrish et al. (2012)
92 integrated Bayesian model averaging and data assimilation to reduce model
93 uncertainty. DeChant and Moradkhani (2014a) combined ensemble data assimilation
94 and sequential Bayesian methods to provide a reliable prediction of seasonal forecast
95 uncertainty. Shi et al. (2014) conducted multiple parameter estimation using
96 multivariate observations via the ensemble Kalman filter (EnKF) for a physically

97 based land surface hydrologic model. However, due to the local complex
98 characteristics of the watershed, some parameters in the hydrologic model may not be
99 clearly identifiable and show slow convergence (Moradkhani et al., 2005b, 2012).
100 Moreover, the same hydrologic model parameter may even show contrary
101 convergence characteristics when different data assimilation methods are used. As
102 shown by Moradkhani et al. (2005a, b), the C_{\max} parameter for the Hymod was
103 identifiable by using particle filter method but unidentifiable by using EnKF. Such
104 unidentifiable parameters would lead to extensive uncertainties in hydrologic
105 forecasts. Moreover, stochastic perturbations are usually added to the model inputs
106 (e.g. precipitation, potential evapotranspiration etc.) and observations (e.g.
107 streamflow) to account for uncertainties in actual measurements. Such random noise
108 would results in uncertainties in model parameters. Consequently, efficient forward
109 uncertainty quantification methods (i.e. from model parameters to model predictions)
110 are still desired for further analyzing the uncertainty in hydrologic predictions. Such
111 methods can reveal the uncertainty evolution and propagation in hydrologic
112 simulation.

113 Previously, Monte Carlo simulations are usually employed to quantify the
114 uncertainty of hydrologic predictions resulting from uncertain model parameters
115 (Knighton et al., 2014; Houska et al., 2014). In such a MC simulation process, model
116 parameters would be sampled from known distributions, and each sample of model
117 parameters would be entered into the hydrologic model to obtain statistics or density
118 estimates of the model predictions. However, with complex hydrologic models such
119 as distributed hydrologic models, this sampling approach is computationally intensive
120 (Herman et al., 2013). The polynomial chaos expansions (PCEs) are effective for
121 uncertainty propagation in stochastic processes, which represent the random variables

122 through polynomial chaos basis and obtain the unknown expansion coefficients by the
123 Galerkin technique or probabilistic collocation method (PCM) (Li and Zhang, 2007;
124 Shi et al., 2009). The PCE-based methods have been widely used for uncertainty
125 quantification of subsurface flow simulation in porous media (Li and Zhang, 2007;
126 Shi et al., 2009), water quality modelling (Zheng et al., 2011), vehicle dynamics
127 (Kewlani et al., 2012), mechanical systems (Blanchard, 2010), and so on. Fan et al.
128 (2015c) integrated PCM into a hydrologic model for exploring the uncertainty
129 propagation in hydrologic simulation, but it is only suitable for quantifying
130 uncertainty of hydrologic models with specific distributions for model parameters
131 (e.g. uniform, normal). However, in real-world hydrologic simulation, the posterior
132 distributions of model parameters, after calibration through probabilistic estimation
133 approaches, may be arbitrary.

134 In this study, a coupled ensemble filtering and probabilistic collocation (EFPC)
135 method is proposed for uncertainty quantification of hydrologic models. In EFPC, the
136 posterior distributions of model parameters will be approximated through EnKF; the
137 obtained posterior distributions will be used as inputs for the probabilistic collocation
138 method, in which PCEs will be constructed to connect the model parameters with the
139 model responses. Such PCEs will reflect the uncertainty propagation between model
140 parameters and its outputs. Therefore, the proposed EFPC will enable improved
141 quantification of uncertainties existing in hydrologic predictions, model parameters,
142 inputs and their interrelationships, and further reveal the uncertainty evolution
143 through the obtained PCEs. Furthermore, a Gaussian anamorphosis (GA) approach
144 will be presented to convert the obtained posterior distributions into standard normal
145 random variables, which can be directly used as the inputs for PCM. The proposed

146 approach will be applied to the Xiangxi River basin based on a conceptual rainfall-
147 runoff model. The Xiangxi River basin, located in the Three Gorges Reservoir area of
148 China, is one of the main tributaries in Hubei Province, with a draining area of about
149 3,200 km². The Hymod, which has been used in many catchments, will be employed
150 in this study (van Delft, 2007; Wang et al., 2009; Dechant and Moradkhani, 2012;
151 Moradkhani et al., 2012). This application will help demonstrate the strength and
152 applicability of the proposed methodology.

153

154 **2. Methodology**

155 **2.1. Ensemble Kalman Filter**

156 The data assimilation methods have attracted increasing attention from
157 hydrologists for exploring more accurate hydrological forecasts based on real-time
158 observations (Moradkhani et al., 2005a; Weerts and El Serafy, 2005; Wang et al.,
159 2009; DeChant and Moradkhani, 2011a,b; Plaza Guingla et al., 2013). Sequential data
160 assimilation is a general framework where system states and parameters are
161 recursively estimated/corrected when new observations are available. In a sequential
162 data assimilation process, the evolution of the simulated system states can be
163 represented as follows:

$$164 \quad x_t^- = f(x_{t-1}^+, u_t, \theta) + \omega_t \quad (1)$$

165 where f is a nonlinear function expressing the system transition from time $t-1$ to t , in
166 response to model input vectors x_{t-1}^+ , u_t and θ ; x_{t-1}^+ is the analyzed (i.e. posteriori)
167 estimation (after correction) of the state variable x at time step $t-1$; x_t^- is the
168 forecasted (i.e. priori) estimation of the state variable x at time step t ; θ represents

169 time-invariant vectors, and ω_t is considered as process noise.

170 When new observations are available, the forecasted states can be corrected
171 through assimilating the observations into the model, based on the output model
172 responding to the state variables and parameters. The observation output model can be
173 written as:

$$174 \quad \tilde{y}_t = h(\tilde{x}_t, \theta) + v_t \quad (2)$$

175 where h is the nonlinear function producing forecasted observations; v_t is the
176 observation noise.

177 The essential methods for states updating are based on Bayesian analysis, in
178 which the probability density function of the current state given the observations is
179 approximated by the recursive Bayesian law:

$$180 \quad p(x_t, \theta_t | y_{1:t}) = \frac{p(y_t | x_t, \theta_t) p(x_t, \theta_t | y_{1:t-1})}{p(y_t | y_{1:t-1})} \quad (3)$$

181 where $p(x_t, \theta_t | y_{1:t-1})$ represents the prior information; $p(y_t | x_t, \theta_t)$ is the
182 likelihood; $p(y_t | y_{1:t-1})$ represents the normalizing constant. If the model is assumed
183 to be Markovian, the prior distribution can be estimated via the Chapman-
184 Kolmogorov equation:

$$185 \quad p(x_t, \theta_t | y_{1:t-1}) = \int p(x_t, \theta_t | x_{t-1}, \theta_{t-1}) p(x_{t-1}, \theta_{t-1} | y_{1:t-1}) dx_{t-1} d\theta_{t-1} \quad (4)$$

186 Similarly, the normalizing constant $p(y_t | y_{1:t-1})$ can be obtained as follows:

$$187 \quad p(y_t | y_{1:t-1}) = \int p(y_t | x_t, \theta_t) p(x_t, \theta_t | y_{1:t-1}) dx_t d\theta_t \quad (5)$$

188 The optimal Bayesian solutions (i.e. equations (3) and (4)) are difficult to
189 determine since the evaluation of the integrals might be intractable (Plaza Guingla et
190 al., 2013). Consequently, approximate methods are applied to treat above issues.

191 Ensemble Kalman Filter (EnKF) and particle filter (PF) are the two widely used
192 methods, in which EnKF can recursively result in optimal estimation for linear
193 dynamic models with Gaussian uncertainties, and PF is suitable for non-Gaussian
194 nonlinear dynamical models (Xie and Zhang, 2013). Particularly, the PF can provide a
195 more accurate update for model states and parameters by adjusting the
196 hyperparameters (e.g., observation perturbation characteristics) based on the
197 observations and ensemble predictions, which avoid excessive adjustment of the
198 ensemble spread while still allowing for a relatively quick response when
199 observations fall outside the prediction bound (Moradkhani, 2008; Leisenring and
200 Moradkhani, 2012). The central idea of EnKF and PF is to quantify the probability
201 density functions (PDF) of model states by a set of random samples. The difference
202 between these two methods lies in the way of recursively generating an approximation
203 for a state PDF (Weerts and EI Serafy, 2005). In EnKF, the distributions are
204 considered to be Gaussian. The Monte Carlo approach is applied to approximate the
205 error statistics and compute the Kalman gain matrix for updating model parameters
206 and state variables.

207 Consider a general stochastic dynamic model with the transition equations of the
208 system state expressed as:

$$209 \quad x_{t+1,i}^- = f(x_{t,i}^+, u_{t,i}, \theta_{t+1,i}^-) + \omega_{t,i}, \quad i = 1, 2, \dots, ne \quad (6)$$

210 where x_t is the states vector at time t ; θ is the system parameters vector assumed to be
211 known and time invariant; the superscript “-” indicates the “forecasted” sates; the
212 superscript “+” indicates the “analyzed” states; ne represents the number of
213 ensembles; u_t is the input vector (deterministic forcing data); f represents the model

214 structure; ω_t is the model error term, which follows a Gaussian distribution with zero
 215 mean and covariance matrix Σ_t^m . For the evolution of the parameters, it is assumed
 216 that the parameters follow a random walk presented as:

$$217 \quad \theta_{t+1,i}^- = \theta_{t,i}^+ + \tau_{t,i}, \quad \tau_{t,i} \sim N(0, \Sigma_t^\theta) \quad (7)$$

218 Prior to update of the model states and parameters, an observation equation is applied
 219 to transfer the states into the observation space, which can be characterized as:

$$220 \quad y_{t+1,i}^- = h(x_{t+1,i}^-, \theta_{t+1,i}^-) + v_{t+1,i}, \quad v_{t+1,i} \sim N(0, \Sigma_{t+1}^y) \quad (8)$$

221 where y_{t+1} is the observation vector at time $t+1$; h is the measurement function
 222 relating the state variables and parameters to the measured variables; $v_{k+1,i}$ reflects the
 223 measurement error, which is also assumed to be Gaussian with zero mean and

224 covariance matrix Σ_{t+1}^y . The model and observation errors are assumed to be

225 uncorrelated, i.e. $E[\omega_t v_{t+1}^T] = 0$. After the prediction is obtained, the posterior states

226 and parameters are estimated with the Kalman update equations as follows (DeChant
 227 and Moradkhani, 2012):

$$228 \quad x_{t+1,i}^+ = x_{t+1,i}^- + K_{xy} [y_{t+1} + \varepsilon_{t+1,i} - y_{t+1,i}^-] \quad (9)$$

$$229 \quad \theta_{t+1,i}^+ = \theta_{t+1,i}^- + K_{\theta y} [y_{t+1} + \varepsilon_{t+1,i} - y_{t+1,i}^-] \quad (10)$$

230 where y_t is the observed values; $\varepsilon_{t,i}$ represents the observation errors; K_{xy} and $K_{\theta y}$ are
 231 the Kalman gains for states and parameters, respectively (DeChant and Moradkhani,
 232 2012):

$$233 \quad K_{xy} = C_{xy} (C_{yy} + R_t)^{-1} \quad (11)$$

$$234 \quad K_{\theta y} = C_{\theta y} (C_{yy} + R_t)^{-1} \quad (12)$$

235 Here C_{xy} is the cross covariance of the forecasted states $x_{t+1,i}^-$ and the forecasted

236 output $\bar{y}_{t+1,i}$; $C_{\theta y}$ is the cross covariance of the parameter ensembles $\bar{\theta}_{t+1,i}$ with the
237 predicted observation $\bar{y}_{t+1,i}$; C_{yy} is the variance of the predicted observation; R_t is the
238 observation error variance at time t .

239

240 **2.2. Probabilistic Collocation Method (PCM)**

241 2.2.1. Polynomial chaos expression (PCE)

242 For a system dynamic model, its outputs are correlated to its input fields. In
243 terms of random characteristics in model inputs, the outputs can be characterized by a
244 nonlinear function with respect to the set of random variables. Polynomial chaos (PC)
245 methods are usually applied to express the evolution of uncertainty in a dynamic
246 system with random inputs. The PC method was first introduced by Wiener (1938),
247 where the model stochastic process is decomposed by Hermite polynomials in terms
248 of Gaussian random variables. The polynomial chaos expansion (PCE) can be seen as
249 a mathematically optimal way to construct and obtain a model response surface in the
250 form of a high-dimensional polynomial to uncertain model parameters (Oladyshkin
251 and Nowak, 2012). This technique includes representing the system outputs through a
252 polynomial chaos basis of random variables which are used to represent input
253 stochasticity, and deriving the unknown expansion coefficients using intrusive (e.g.
254 stochastic Galerkin technique) and non-intrusive (e.g. probabilistic collocation
255 method) approaches. The original PCE is based on Hermite polynomials, which are
256 optimal for normally distributed random variables (Oladyshkin and Nowak, 2012).
257 However, for non-Gaussian random input variables (e.g. Gamma and uniform), the
258 convergence of Hermite polynomial expansion is not optimal (Xiu and Karniadakis,
259 2003). Xiu and Karniadakis (2002) proposed generalized polynomial chaos expansions
260 for non-Gaussian distributions. The general polynomial chaos expansion can be written

261 in the form:

$$262 \quad y = a_0 + \sum_{i_1=1}^n a_{i_1} \Gamma_1(\zeta_{i_1}) + \sum_{i_1=1}^n \sum_{i_2=1}^{i_1} a_{i_1 i_2} \Gamma_2(\zeta_{i_1}, \zeta_{i_2}) + \sum_{i_1=1}^n \sum_{i_2=1}^{i_1} \sum_{i_3=1}^{i_2} a_{i_1 i_2 i_3} \Gamma_3(\zeta_{i_1}, \zeta_{i_2}, \zeta_{i_3}) + \dots \quad (13)$$

263 where y is the output and $\Gamma_p(\zeta_{i_1}, \zeta_{i_2}, \dots, \zeta_{i_p})$ are the polynomial chaos of order p in terms

264 of the multi-dimensional random variables $\{\zeta_{i_k}\}_{k=1}^M$. For standard normal variables, the

265 Hermite polynomial will be used, which is expressed as:

$$266 \quad \Gamma_p(\zeta_{i_1}, \zeta_{i_2}, \dots, \zeta_{i_p}) = (-1)^p e^{1/2 \zeta^T \zeta} \frac{\partial^M}{\partial \zeta_{i_1} \partial \zeta_{i_2} \dots \partial \zeta_{i_p}} e^{-1/2 \zeta^T \zeta} \quad (14)$$

267 where $(\zeta_{i_1}, \zeta_{i_2}, \dots, \zeta_{i_p})$ (ζ is the vector form) are the standard normal random variables

268 (SRV). The polynomial with an order greater than one has zero mean; polynomials of

269 different orders are orthogonal to each other, and so are polynomials of the same order

270 but with different arguments (Huang et al., 2007).

271 Previous studies have demonstrated that accurate approximations can be

272 obtained through a truncated PCE with only low order terms (Lucas and Prinn, 2005;

273 Li and Zhang, 2007; Shi et al., 2009; Zheng et al., 2011). The computational

274 requirement increases as the order of PCE increases. The total number of the

275 truncated terms N for PCE is related to the dimension of the random variables M and

276 the highest order of the polynomial p :

$$277 \quad N = \frac{(M+p)!}{M!p!} \quad (15)$$

278 Table 1 contains some explicit values of N for given dimension of the random

279 variables M and the order of the polynomial p . Thus Equation (10) can be written

280 simply as:

$$281 \quad y = \sum_{j=0}^{M-1} c_j \Psi_j(\zeta_i) \quad (16)$$

282 in which there is a one-to-one mapping between $\Gamma_p(\zeta_{i_1}, \zeta_{i_2}, \dots, \zeta_{i_p})$ and $\Psi_j(\zeta_i)$, and
 283 also between c_j and $a_{i_1 i_2 \dots i_p}$. For instance, the 2-order 2-dimensional PCE can be
 284 expressed as: $y = c_0 + c_1 \zeta_1 + c_2 \zeta_2 + c_3(\zeta_1^2 - 1) + c_4(\zeta_2^2 - 1) + c_5 \zeta_1 \zeta_2$; the 2-order 3-
 285 dimensional PCE can be written as: $y = c_0 + c_1 \zeta_1 + c_2 \zeta_2 + c_3 \zeta_3 + c_4(\zeta_1^2 - 1) + c_5(\zeta_2^2 -$
 286 $1) + c_6(\zeta_3^2 - 1) + c_7 \zeta_1 \zeta_2 + c_8 \zeta_1 \zeta_3 + c_9 \zeta_2 \zeta_3$.

287

288 -----

289 Place Table 1 Here

290 -----

291

292 2.2.2. Selection of collocation points for PCM

293 The basic idea of the probabilistic collocation method (PCM) is to let the
 294 polynomial chaos expansion (PCE) in terms of random inputs to be the same as the
 295 model simulation results at selected collocation points. The collocation points can be
 296 specified by various algorithms. In this study, the collocation points are derived from
 297 combinations of the roots of a Hermite polynomial with one order higher than the
 298 order of PCE. For a 2-order PCE, the collocation points are combinations of the roots
 299 of the 3-order Hermite polynomial $H_3(\zeta) = \zeta^3 - 3\zeta$, which are $(-\sqrt{3}, 0, \sqrt{3})$. For
 300 example, for a 2-order 2-dimensional PCE expressed as: $y = y = c_0 + c_1 \zeta_1 + c_2 \zeta_2 +$
 301 $c_3(\zeta_1^2 - 1) + c_4(\zeta_2^2 - 1) + c_5 \zeta_1 \zeta_2$, the collocation points $(\zeta_{1,i}, \zeta_{2,i})$ are chosen from the
 302 combinations of the three roots of the 3-order Hermite polynomial, which consists of
 303 a total of 9 collocation points which are expressed as: $(-\sqrt{3}, -\sqrt{3}), (-\sqrt{3}, 0), (-\sqrt{3},$
 304 $\sqrt{3}), (0, -\sqrt{3}), (0, 0), (0, \sqrt{3}), (\sqrt{3}, -\sqrt{3}), (\sqrt{3}, 0), (\sqrt{3}, \sqrt{3})$. For a 3-order PCE,
 305 the collocation points are chosen based on the values of $\pm\sqrt{3 \pm \sqrt{6}}$, which are the

306 roots of the 4-order Hermite polynomial $H_4(\zeta) = \zeta^4 - 6\zeta^2 + 3$. Furthermore, the
307 selection is also expected to capture regions of high probability (Huang et al., 2007;
308 Li and Zhang, 2007). The value of zero has the highest probability for a standard
309 normal random variable, and thus the collocation points for 3-order PCE are the
310 combinations of $(0, \pm\sqrt{3 \pm \sqrt{6}})$. The potential collocation points for the 2- and 3-
311 order PCEs with two standard random variables are presented in Table 2.

312

313 -----

314 Place Table 2 Here

315 -----

316

317 2.2.3. Unknown Parameter Estimation

318 Probabilistic collocation method (PCM) is implemented through approximating a
319 model output with a polynomial chaos expansion (PCE) in terms of random inputs
320 (Zheng et al., 2011). The unknown coefficients contained in the expansion can be
321 determined based on model simulations at selected collocation points (each
322 collocation point is a realization of the random inputs). Generally, there are two
323 methods to obtain the unknown coefficients in PCE. The first one is to solve a linear
324 equations system expressed as: $N \times a = f$, where N is a space-independent matrix of
325 dimension $P \times P$, consisting of Hermite polynomials evaluated at the selected
326 collocation points; a is the unknown coefficient vector of the PCE; f is the realization
327 of the simulation model at the selected collocation points. However, such a method
328 may be unstable and the approximation results are highly dependent on the selection
329 of the collocation points (Huang et al., 2007). Consequently, Huang et al. (2007)
330 modified the collocation method to employ more collocation points than the number

331 of unknown coefficients through a regression based method. In this study, we will
332 employ the regression-based method to obtain the unknown coefficients in PCE. The
333 detailed process for PCM method is illustrated in Figure 1.

334 -----
335 Place Figure 1 here

336 -----

337

338 **2.3. Uncertainty Quantification for the Hydrological Model based on Coupled** 339 **Ensemble Filtering and Probabilistic Collocation (EFPC) Method**

340 Hydrologic models contain parameters that cannot be measured directly, and
341 must therefore be estimated using measurements of the system inputs and outputs
342 (Vrugt et al., 2005). Sequential data assimilation (SDA) is a class of methods that
343 provide a general framework for explicitly dealing with input, output and model
344 structural uncertainties. Of these SDA techniques, the ensemble Kalman filter (EnKF)
345 is one of the most widely used methods in hydrologic community (Moradkhani et al.,
346 2005a; DeChant and Moradkhani, 2012; Leisenring and Moradkhani, 2011; Li et al.,
347 2013; Liu et al., 2012). The EnKF method is much more effective for reducing
348 uncertainty and characterizing posterior distributions for model parameters as it can
349 merge the observations and model outputs to improve the model predictions, and
350 further characterize the initial condition of uncertainty of the catchment. However,
351 uncertainty propagation and evolution from model parameters to model outputs can
352 hardly be revealed just merely through EnKF. Consequently, in this study, we will
353 integrate the ensemble Kalman filter (EnKF) and the probabilistic collocation
354 methods (PCM) into a general framework to quantify the uncertainty of hydrological
355 predictions. The posterior probability distributions of model parameters are estimated

356 by EnKF, and the uncertainty propagation and evolution from uncertainty parameters
357 to model outputs are further characterized by PCM.

358

359 2.3.1. Gaussian Anamorphosis Transformation for Non-Gaussian Distributions

360 When the polynomial chaos expansion (PCE) is applied to express the evolution
361 of uncertainty in a dynamic system with random inputs, those random inputs should
362 be transformed to random variables with specific distributions. For example, as
363 proposed in Equation (14), for the stochastic process decomposed by Hermite
364 polynomials, the random inputs should be first expressed through the standard
365 Gaussian random variables. The EnKF method can continuously update the states and
366 parameters in the model when new measurements become available. After the EnKF
367 update process, the distributions of model parameters can hardly be normally
368 distributed, even though their prior distributions are assumed to be normal. Moreover,
369 the distributions of the updated parameters can hardly be expressed through some
370 specific distributions (e.g. gamma, uniform, etc.) in many cases.

371 Consequently, in order to further quantify the inherent uncertainty of the
372 hydrologic model after the data assimilation process, transformation techniques
373 should applied to convert the posterior distributions of the updated parameters into
374 standard Gaussian distributions. In this study, a nonlinear, monotonic transform
375 technique known as Gaussian anamorphosis (GA), will be applied to transform the
376 posterior distributions of model parameters to standard normal distributions. For the
377 original random variable x and the transformed random variable $y = f(x)$, the idea of
378 GA is to find a function f to define a change of the variable (anamorphosis) such that
379 the random variable y obeys a standard Gaussian distribution. Such a transformation
380 technique was applied in biogeochemical ocean model (Simon and Bertino, 2009),

381 physical-biogeochemical ocean model (Béal et al., 2010) and subsurface hydraulic
382 tomography model (Schöniger et al., 2012). In this study, the GA method will be
383 applied to combine the EnKF and PCM method together to quantify the uncertainty of
384 hydrologic models.

385 Consider an arbitrarily distributed variable y and its Gaussian transform variable
386 z ; they can be linked through their cumulative distribution functions (CDFs) as
387 follows:

$$388 \quad z = G^{-1}(F(y)) \quad (17)$$

389 where $F(y)$ is the empirical CDF of y , G is the theoretical standard normal CDF of z .
390 since G is monotonously increasing, the inverse G^{-1} exists. Equation (17) is called
391 Gaussian anamorphosis function.

392 Following the method proposed by Johnson and Wichern (1988), the empirical
393 CDF of y can be obtained based on its sample values as follows:

$$394 \quad F_j = \frac{j-0.5}{N} \quad (18)$$

395 where j are the rank of the sample value of y ; N is the sample size of y (rendered as
396 the ensemble size of EnKF in this study). From Equations (17) and (18), the sample
397 values of the Gaussian transform variable z can be obtained, which correspond to the
398 sample values of y . Also, the sample range of z can be determined as follows:

$$399 \quad z_{\min} = G^{-1}\left(\frac{1-0.5}{N}\right) \quad (19)$$

$$400 \quad z_{\max} = G^{-1}\left(\frac{N-0.5}{N}\right) \quad (20)$$

401

402 2.3.2. The Detailed Procedures of the EFPC method

403 The process of the proposed EFPC method mainly involves two components: the
404 EnKF update procedures for uncertainty reduction and the PCM procedures for

405 uncertainty quantification. The detailed process of EFPC includes the following steps:

406 *Step (1)*. Model state initialization: initialize N_x -dimensional model state variables and

407 parameters for ne samples: $x_{t,i}^-$, $i = 1, 2, \dots, ne$, $x \in R^{N_x}$; $\theta_{t,i}$, $i = 1, 2, \dots, ne$, $\theta \in R^{N_\theta}$.

408 *Step (2)*. Model state forecast step: propagate the ne state variables and model

409 parameters forward in time using model operator f :

$$410 \quad x_{t+1,i}^- = f(x_{t,i}^-, u_{t,i}, \theta_{t+1,i}^-) + \omega_{t+1,i}, \quad \omega_{t+1,i} \sim N(0, \Sigma_t^m), \quad i = 1, 2, \dots, ne$$

411 *Step (3)*. Observation simulation: use the observation operator h to propagate the

412 model state forecast:

$$413 \quad y_{t+1,i}^- = h(x_{t+1,i}^-, \theta_{t+1,i}^-) + v_{t+1,i}, \quad v_{t+1,i} \sim N(0, \Sigma_{t+1}^y), \quad i = 1, 2, \dots, ne$$

414 *Step (4)*. Parameters and states updating: update the parameters and states via the

415 EnKF updating equations:

$$416 \quad x_{t+1,i}^+ = x_{t+1,i}^- + K_{xy} [y_{t+1,i} + \varepsilon_{t+1,i} - y_{t+1,i}^-]$$

$$417 \quad \theta_{t+1,i}^+ = \theta_{t+1,i}^- + K_{\theta y} [y_{t+1,i} + \varepsilon_{t+1,i} - y_{t+1,i}^-]$$

418 *Step (5)* Parameter perturbation: take parameter evolution to the next stage through

419 adding small stochastic error around the sample:

$$420 \quad \theta_{t+2,i}^+ = \theta_{t+1,i}^+ + \tau_{t+1,i}, \quad \tau_{t+1,i} \sim N(0, \Sigma_{t+1}^\theta)$$

421 *Step (6)*. Check the stopping criterion: if measurement data is still available in the

422 next stage, $t = t + 1$ and return to step 2; otherwise, continue to the next step.

423 *Step (7)*. Convert the parameter θ into standard Gaussian variables through GA.

424 *Step (8)*. Approximate the outputs of interest using the polynomial chaos expansion in

425 terms of the standard Gaussian variables.

426 *Step (9)*. Select the collocation points according to the dimensions of the stochastic

427 vector and the order of the applied polynomial chaos expansion.

428 *Step (10)*. Determine the unknown coefficients in the polynomial expansion through

429 statistical regression techniques.

430 *Step* (11). Evaluate the inherent statistical properties of the outputs stemming from the
431 uncertainty of the parameters.

432

433 **3. Experimental Setup**

434 **3.1. The Conceptual Hydrologic Model**

435 The Hymod, which is a well-known conceptual hydrologic model, will be used in this
436 study. Hymod is a non-linear rainfall-runoff conceptual model which can be run in a
437 minute/hour/daily time step (Moore, 1985). The general concept of the model is based
438 on the probability distribution of soil moisture modeling proposed by Moore (1985,
439 2007). In Hymod the catchment is considered as an infinite amount of points each of
440 which has a certain soil moisture capacity denoted as c [L] (Wang et al., 2009). Soil
441 moisture capacities vary within the catchment due to spatial variability such as soil
442 type and depth and a cumulative distribution function (CDF) is proposed to describe
443 such variability, expressed as (Moore, 1985, 2007):

$$444 \quad F(c) = 1 - \left[1 - \frac{c}{C_{max}} \right]^{b_{exp}}, \quad 0 \leq c \leq C_{max} \quad (21)$$

445 where C_{max} [L] is the maximum soil moisture capacity within the catchment and b_{exp}
446 [-] is the degree of spatial variability of soil moisture capacities and affects the shape
447 of the CDF.

448

449 As shown in Figure 2, the Hymod conceptualizes the rainfall-runoff process through a
450 nonlinear rainfall excess model connected with two series of reservoirs (three
451 identical quick-flow tanks representing the surface flow in parallel with a slow-flow
452 tank representing the groundwater flow). The Hymod has five parameters to be

453 calibrated: (i) the maximum storage capacity in the catchment C_{max} , (ii) the degree of
454 spatial variability of the soil moisture capacity within the catchment, (iii) the factor
455 partitioning the flow between the two series of linear reservoir tanks α , (iv) the
456 residence time of the linear quick-flow tank R_q , and (v) the residence time of the slow-
457 tank R_s . The model uses two input variables: mean areal precipitation, P (mm/day),
458 and potential evapotranspiration, ET (mm/day).

459

460 -----

461 Place Figure 2 Here

462 -----

463 **3.2. Site Description**

464 The Xiangxi River basin, located in the Three Gorges Reservoir area (Figure 3),
465 China, is selected to demonstrate the effectiveness of the proposed forecasting
466 algorithm. The Xiangxi River is located between $30.96 \sim 31.67^{\circ}\text{N}$ and $110.47 \sim$
467 111.13°E in the Hubei part of the China Three Gorges Reservoir (TGR) region, with a
468 draining area of approximately $3,200 \text{ km}^2$. The Xiangxi River originates in the
469 Shennongjia Nature Reserve with a main stream length of 94 km and a catchment area
470 of $3,099 \text{ km}^2$ and is one of the main tributaries of the Yangtze River (Han et al., 2014;
471 Yang and Yang, 2014; Miao et al., 2014). The watershed experiences a northern
472 subtropical climate. The annual precipitation is about 1,100 mm and ranges from 670
473 to 1,700 mm with considerable spatial and temporal variability (Xu et al., 2010;
474 Zhang et al., 2014). The main rainfall season is from May through September, with a

475 flooding season from July to August. The annual average temperature in this region is
476 15.6 °C and ranges from 12 °C to 20 °C.

477 -----

478 Place Figure 3 here

479 -----

480

481 **3.3. Synthetic Data Experiment**

482 In this study, a synthetic case will be initially applied to demonstrate the applicability
483 of the EFPC method in quantifying prediction uncertainty. For the synthetic
484 experiment, “truth” is defined when the model is run for a set of meteorological and
485 initial conditions (Moradkhani, 2008). In detail, the model parameter values are
486 predefined as the “true” values presented in Table 3. The model inputs, including the
487 potential evapotranspiration, ET (mm/day), and mean areal precipitation, P (mm/day),
488 are the observed data collected at Xingshan Hydrologic Station (110°45’0’’ E,
489 31°13’0’’ N) on the main stream of the Xiangxi River. These data are provided by the
490 Water Conservancy Bureau of Xiangshan County. Using these model inputs and
491 parameter values, the “true states” and “true streamflow observations” can be
492 generated by running Hymod. Such generated streamflow values are considered as the
493 observations in the EnKF updating process. Moreover, as with any data assimilation
494 framework, it is necessary to assume error values for any quantity that contains
495 uncertainties (DeChant and Moradkhani, 2012). In the synthetic experiment, the
496 model structure is assumed to be perfect. Thus, random perturbations would be added
497 to precipitation and potential evapotranspiration (ET) observations to account for their
498 uncertainties. In this study, these random perturbations are assumed to be normally
499 distributed with the mean values being 0 and the standard errors being proportional to

500 the magnitude of true values. The proportional coefficients for precipitation, potential
501 evapotranspiration, and streamflow observations are all set to be 0.1. This means that
502 precipitation, ET, and streamflow observations are assumed to have normal
503 distributions with relative errors of 10%. However the study proposed by DeChant
504 and Moradkhani (2011a; 2011b) showed that the log-norm perturbation for
505 precipitation is more appropriate. The comparison among norm and log-norm
506 perturbation for precipitation will be conducted in the subsequent real-case study.

507

508 -----

509 Place Table 3 Here

510 -----

511 3.4. Evaluation Criteria

512 To evaluate the performance of the proposed EFPC approach, some indices are
513 introduced. In detail, root-mean-square error (RMSE), the Nash-Sutcliffe efficiency
514 (NSE) coefficient and the percent bias (%BIAS) will be employed to evaluate the
515 performance of the proposed method, which are expressed as follows:

$$516 \quad RMSE = \sqrt{\frac{1}{N} \sum_{i=1}^N (Q_i - P_i)^2} \quad (22)$$

$$517 \quad NSE = 1 - \frac{\sum_{i=1}^N (Q_i - P_i)^2}{\sum_{i=1}^N (Q_i - \bar{Q})^2} \quad (23)$$

$$518 \quad PBIAS = \frac{\sum_{i=1}^N (Q_i - P_i) * 100}{\sum_{i=1}^N Q_i} \quad (24)$$

519

520 where N is the total number of observations (or predictions), Q_i are the observed
521 values, P_i are the estimated values, and \bar{Q} is the mean of all observed and estimated
522 values

523

524 **4. Results Analysis of Synthetic Experiment**

525 **4.1. Uncertainty Characterization of Hymod through EnKF**

526 To demonstrate the capability of EnKF in model parameter estimation and
527 uncertainty reduction, the five parameters of Hymod (i.e. C_{max} , b_{exp} , α , R_q , R_s) are
528 initialized to be varied within predefined intervals, as presented in Table 3. The
529 ensemble size in this study was set to be 50. This ensemble size is set based on the
530 conclusion from Yin et al. (2015). They tested the optimal ensemble size of EnKF in
531 sequential soil moisture data and found that the standard deviation decreases sharply
532 with ensemble size increasing when the ensemble size was less than 10, and this
533 tendency was to slow down when the ensemble size was greater than 10 (Yin et al.,
534 2015). Particularly, for larger ensemble sizes, the error variance did not decrease
535 much further, suggesting that the EnKF estimates at the final times might not
536 converge to the optimal smoothing solution when the ensemble size became too large
537 (Yin et al., 2015). The random perturbation for parameter evolution in Equation (7) is
538 set to have a normal distribution with a relative error of 10%. The initial samples of
539 the five parameters are uniformly sampled from those predefined intervals and the
540 total data assimilation steps would be one year (i.e. 365 days).

541 Figure 4 shows the comparison between the ensembles of the forecasted
542 streamflow and the synthetic-generated true discharge. The results indicate that the
543 ensemble means of streamflow predictions can track the observed discharge data. The
544 ranges formulated by 5 and 95% percentiles (i.e. 90% confidence intervals) of

545 streamflow predictions can adequately bracket the observations. Figure 5 depicts the
546 evolution of the sampled marginal posterior distributions for the five parameters of
547 Hymod during the EnKF assimilation period. From Figure 5, it is observed that b_{exp} ,
548 α , R_q and R_s are identifiable, while in comparison, the C_{max} parameter is less
549 identifiable than the other four parameters. This means that the marginal distribution
550 of C_{max} exhibits considerable uncertainty and move intermittently throughout the
551 feasible parameter space. For b_{exp} , α , R_q and R_s , one year discharge observations are
552 deemed sufficient to estimate their values. Table 3 presents the final fluctuating
553 intervals for these five parameters after one year data assimilation period. It is
554 indicated that the EnKF method estimated C_{max} , b_{exp} , R_s accurately, while there are
555 small differences between the true values and the final estimated intervals for α and
556 R_q . The extensive uncertainty of C_{max} indicates that, in this synthetic experiment, the
557 C_{max} is low sensitivity to the model prediction performance.

558

559 -----

560 Place Figures 4 and 5 Here

561 -----

562

563 In this study, we set the ensemble size to be 50. To confirm the effectiveness of this
564 ensemble size, we compare the performance of EnKF under different ensemble sizes.
565 In detail, six ensemble size scenarios are assumed, and under each scenario, the
566 synthetic experiment is run 10 times. The results of the mean values of NSE, RMSE,
567 and PBIAS are presented in Table 4. The results show that as the increase in ensemble
568 size, the performance of EnKF would not be improved significantly; conversely,

569 EnKF performed slightly worse as ensemble size larger than 150. This may because
570 that the EnKF estimates at the final times might not converge to the optimal
571 smoothing solution when the ensemble size became too large (Yin et al., 2015).
572 Therefore, in this study, the ensemble size being 50 seems to be appropriate in this
573 study.

574

575 -----

576 Place Table 4 Here

577 -----

578

579 EnKF can merge the observations and model outputs to improve the model
580 predictions, and further characterize the initial condition uncertainty. The posterior
581 probability distributions for model parameters can be estimated through EnKF, and
582 the uncertainty in model parameters can be significantly reduced. However, as
583 presented in Table 3, the parameters of Hymod still contain some uncertainties. These
584 uncertainties may result from random errors in the precipitation, potential
585 evaporation, streamflow observation and model prediction. Consequently, further
586 exploration would be required to characterize uncertainty propagation in hydrologic
587 simulation and analyze the inherent statistic characteristics of the hydrologic
588 predictions after data assimilation.

589

590 **4.2. Uncertainty Quantification of Hymod through the Probabilistic Collocation Method.**

591 In this study, the Hermite polynomial chaos expansion is employed to quantify
592 the evolution of uncertainty in Hymod stemming from the uncertain parameters.

593 Consequently, the posterior distributions of model parameter estimated by EnKF
594 would be firstly converted into standard Gaussian distribution. As presented in Table
595 3, after the data assimilation process through EnKF, there is still some extent of
596 uncertainty existing in the five parameters of Hymod. Since the value of R_q changes
597 within a very small interval (i.e. [0.75, 0.76]), it will be considered to be deterministic
598 in further uncertainty quantification through PCM. The other four parameters (i.e.
599 C_{max} , b_{exp} , α , R_s) are transformed to standard Gaussian distributions according to GA
600 method proposed by Equations (17) - (19). Figure 6 shows the histogram of original
601 data, empirical anamorphosis function, histogram of transformed data, and normal
602 probability plot of transformed data for C_{max} . Obviously, after transformation through
603 GA, the sample values of C_{max} are well fitted to a standard Gaussian distribution.
604 Similarly, the posterior distributions of b_{exp} , α , R_s can also be converted to standard
605 Gaussian distributions through the GA method. These transformed data can be
606 introduced into the PCM method to further quantify the uncertainty of Hymod.

607

608 -----

609 Place Figure 6 Here

610 -----

611

612 The 2-order polynomial chaos expansion (PCE) is employed to quantify the
613 uncertainty in the Hymod predictions. Since there are four parameters in Hymod (i.e.
614 C_{max} , b_{exp} , α , R_s), the PCE used to represent the output of interest (i.e. streamflow)
615 would be four-dimensional and two order. The detailed polynomials of the 4-
616 dimensional 2-order PCE are expressed by Equation (16). There are total of 15
617 unknown coefficients in this 4-dimensional 2-order PCE. The potential collocation

618 points are obtained through combining the roots (i.e. $(-\sqrt{3}, 0, \sqrt{3})$) of the 3-order
619 Hermite polynomial $H_3(\zeta) = \zeta^3 - 3\zeta$. For a 4-dimensional 2-order PCE, there are 81
620 (i.e. 3^4) potential collocation points. For each collocation point, the probability can be
621 obtained through the standard CDF G in Equation (17), and consequently, the
622 corresponding rank j can be calculated through Equation (18). Since j may not be an
623 integer, the original value of C_{max} , b_{exp} , α , or R_s corresponding to the collocation point
624 of ζ would be obtained through linear interpolation method based on the two adjacent
625 original data. In this paper, all the collocation points would be used to establish the
626 linear regression equations and generate the values of unknown coefficients of PCE.
627 Afterward, 2,000 values are independently sampled from the standard Gaussian
628 distribution for ζ_1 , ζ_2 , ζ_3 , and ζ_4 , respectively, and 2,000 realizations would be
629 generated through both the obtained PCE and Hymod. The latter 2,000 realizations
630 obtained through Hymod are considered as Monte Carlo simulation results.

631 Figure 7 shows the comparison for the mean values of the streamflow obtained
632 through 2-order PCE and Monte Carlo (MC) simulation methods. It indicates that the
633 mean values obtained through 2-order PCE are highly identical to the MC simulation
634 results. This means that the 2-order PCE can generally replace the hydrologic model
635 (i.e. Hymod) to reflect the temporal variations for the streamflow. Figure 8 compares
636 the standard deviations of the streamflow, at each time step, obtained through 2-order
637 PCE and MC simulation methods, respectively. It suggests that the standard deviation
638 of 2-order PCE and MC simulation is identical at low uncertain conditions (i.e. low
639 standard deviation values). During the high streamflow periods, the standard deviation
640 obtained by the 2-order PCE would be slightly less than the actual values (i.e. MC
641 results). However, the PCE results would generally fit well with the MC simulation
642 results in both means and standard deviations. As shown in Figure 9, the relative

643 errors between the standard deviations from MC simulation and 2-order PCE
644 prediction results are relatively small, and most of them are located within [-0.10,
645 0.10]. Moreover, Figure 10 shows the comparison between the 90% confidence
646 intervals from the MC simulation and 2-order PCE prediction results. It indicates that
647 the predicted intervals of streamflow from MC simulation and 2-order PCE are highly
648 consistent under the 90% confidence level.

649

650 -----

651 Place Figures 7 to 10 Here

652 -----

653

654 To further compare the accuracy between 2-order PCE and MC simulation
655 results, the detailed statistical characteristics would be analyzed at specific time
656 periods. The specific time periods are selected artificially through screening the mean
657 streamflow values, as shown in Figure 7, over the simulation period so that the low,
658 medium, and high streamflow levels are all considered. Consequently, the streamflow
659 predictions from MC simulation and PCE at the day 23, 145, 181, 182, 218, 350 are
660 chosen, and their inherent statistical properties are further analyzed. These statistical
661 properties, including mean, standard deviation, kurtosis and skewness, are presented
662 in Table 5. The results show that the probability density distributions obtained through
663 2-order PCE would be similar with those obtained by MC simulation. However, the
664 shape of those probability density distributions generated by 2-order PCE would be
665 slightly steeper (i.e. lower standard deviation and higher kurtosis) than those from MC
666 simulation method. For example, at the 181th day, the mean, standard deviation,
667 kurtosis, skewness values obtained by 2-order PCE would be 613.59, 76.32, 3.01,

668 0.23, respectively, while those values generated by MC simulation method would be
669 615.01, 84.43, 2.07, 0.12, respectively. Figure 11 shows the histograms of 2-order
670 PCE and MC simulation results at the selected time periods. In Figure 11, the left
671 column in each subfigure represents the histogram obtained through MC method,
672 while the right one express the histogram obtained by PCE results. It can be seen from
673 Figure 11 that the shapes of the probability distributions obtained by 2-order PCE
674 have similar shapes with those obtained from the MC simulation results. This
675 suggests that the PCE model obtained by the proposed EFPC can be effective to
676 replace the original hydrologic model to characterize the uncertainty in hydrologic
677 predictions.

678

679 -----

680 Place Table 5 and Figure 11 Here

681 -----

682

683 Generally, after the data assimilation process by EnKF, the uncertainty of Hymod
684 would be significantly reduced, and the posterior probability of model parameters
685 would be estimated. The probabilistic collocation method (PCM) can further
686 characterize the uncertainty propagation through establishing a PCE model between
687 the model parameters and model outputs. Such a model can well reveal uncertainty
688 evolution in hydrologic simulations. Even based on the 2-order PCE, the mean and
689 standard deviation values of this PCE model would be consistent with those obtained
690 by MC simulation method. Moreover, the detailed probability densities generated by
691 2-order PCE at each time step would have similar shapes than those obtained through
692 MC simulation method.

693

694 **5. Real Case Study**

695 **5.1. Model Setup**

696

697 A real-case study will be performed to further demonstrate the applicability of
698 the proposed EFPC method in quantifying uncertainty for hydrologic models. This
699 real-case study is set up based on on-site measurements for daily precipitation,
700 potential evapotranspiration, and streamflow discharge from 1991 to 1993 at the
701 Xingshan Hydrologic Station on the Xiangxi River.

702 The EnKF method can quantify model errors, which may be caused by
703 uncertainties in model inputs, structures, and parameter values, by using the variance
704 of streamflow predictions from an ensemble of model realizations (McMillan, 2013).
705 Random perturbations are added to model inputs, outputs, and parameters to reflect
706 their inherent uncertainties. In the synthetic experiment, random perturbations were
707 added to precipitation and potential evapotranspiration (ET) observations, which were
708 normally distributed with standard errors being 10% of the true values. In order to
709 investigate the impact of relative errors on the performance of EnKF, five relative
710 error scenarios would be assumed. In detail, precipitation is assumed to be normally
711 distributed with relative error being 10, 15, 20, 25, and 30% of the true values,
712 respectively, and ET is also normally distributed having the same relative errors. For
713 the streamflow measurements, several studies set the standard deviation of the
714 observed error to be proportional to the true discharge (Dechant and Moradkhai,
715 2012; Moradkhani et al., 2012; Abaze, et al., 2014), while some research works
716 assumed the error to be proportional to the log discharge (Clark et al, 2008; McMillan
717 et al., 2013). In our study, five relative errors would be selected (i.e. 10, 15, 20, 25 and

718 30%) in order to characterize their impacts on the performance of EnKF. Also, these
719 five error scenarios are assumed to account for the uncertainty in the model
720 predictions.

721

722 **5.2. Impact of Stochastic Perturbation on the Performance of EnKF**

723 Table 6 shows the performance of EnKF under different relative error scenarios.
724 The results indicate that the stochastic perturbation can influence the performance of
725 EnKF. In detail, large relative errors may better reflect the uncertainties in the
726 catchment, and thus leading to better model performance. In this study, the
727 performance of EnKF would be improved as the relative error increases from 10% to
728 20%. However, such a trend would not keep going as the relative larger than 20%.
729 Consequently, for the Xiangxi River, the relative error of 20% may be the appropriate
730 stochastic perturbation to account for the uncertainties in the precipitation, potential
731 evapotranspiration and streamflow observation.

732

733 -----

734 Place Table 6 Here

735 -----

736

737 **5.3. Uncertainty Quantification**

738 Based on the EnKF approach, the posterior probabilities of model parameters
739 would be identified. However, uncertainties in hydrologic predictions, stemming from
740 the uncertainties in hydrologic parameters, are still required to be characterized.
741 Previous research works mainly address this issue through the Monte Carlo method,
742 in which random samples are drawn from the posterior distributions of hydrologic

743 parameters to run the original hydrologic model (Lu and Zhang, 2003; Khu and
744 Werner, 2003; Demaria et al., 2007). This approach may be insufficient, especially for
745 complex hydrologic models, which requires a large number of runs to establish a
746 reliable estimate of model uncertainties (Khu and Werner, 2003). Moreover,
747 traditional Monte Carlo method can hardly reveal how these model parameters would
748 affect the uncertainties in model predictions. Therefore, the developed ensemble
749 filtering and probabilistic collocation (EFPC) method can better address the above
750 issues, in which the posterior probabilities of model parameters would be estimated
751 through EnKF and the probabilistic collocation method (PCM) would be further
752 proposed to establish a proxy for the hydrologic model, with respect to the posterior
753 distributions of model parameters, to reveal the uncertainty evolution in the
754 hydrologic simulation.

755 The results in Table 6 show that a relative error of 0.2 may be appropriate to
756 account for the inherent uncertainty in the Xiangxi River. The potential
757 evapotranspiration, streamflow observations, and model predictions are normally
758 distributed with the standard errors being 20% of the true values. For the
759 precipitation, it is first assumed to be normally distributed with a relative error of
760 20%. Based on the proposed EFPC approach, a polynomial chaos expansion (PCE)
761 can be obtained at each time period, which expresses the relationship between the
762 discharge prediction and the uncertain model parameters.

763 Figure 12 shows the comparison between predicting means of hydrologic model
764 and observations as well as PCE results and observations. This figure is obtained
765 under the assumption of normal error distribution for precipitation. Figure 12(a)
766 indicates the mean predictions of hydrologic model and observations. The mean
767 predictions in Figure 12(a) are obtained through Monte Carlos method in which the

768 parameters values of the hydrologic model are sampled based on their posterior
769 probabilities estimated through EnKF. Figure 12(b) shows the mean predictions of
770 PCE and observations. This figure suggests that the predictions from hydrologic
771 model and PCE show similar trend. The mean predictions from both hydrologic
772 model and PCE can well track the observed streamflow data, except some
773 underestimates during some extreme flow periods. To evaluate the performance of
774 hydrologic model and PCE obtained by the proposed EFPC method, the values of
775 RMSE, PBIAS, and NSE are calculated based on the prediction means and
776 observations. Table 7 compares the results of RMSE, PBIAS, and NSE values
777 obtained through the original hydrologic model and PCE. The comparison process is
778 as follows: (i) choosing N samples from the standard Gaussian distribution, (ii)
779 generating the associated parameter values of the hydrologic model based on the
780 relationships between posterior distributions and standard Gaussian distribution
781 established by the GA approach, (iii) running PCE and hydrologic model respectively,
782 (iv) obtaining the evaluation criteria results. The results in Table 7 indicate good
783 performance of hydrologic model and PCE in tracking the streamflow dynamics in the
784 Xiangxi River, with high NSE values and low PBIAS and RMSE values. Particularly,
785 the hydrologic model performs slightly better than the PCE approach. This is because
786 the PCEs generated by the proposed EFPC method is a proxy of the hydrologic
787 model. However, the results in Table 7 suggest that the PCE can adequately represent
788 the hydrologic model. Figure 13 compares the 90% confidence intervals of hydrologic
789 model vs. observations and 90% confidence intervals of PCE predictions vs.
790 observations. This figure shows that 90% prediction intervals from hydrologic model
791 and PCE can encompass most observations.

792 -----

793 Place Table 7 and Figures 12 and 13 Here

794 -----

795

796 As recommended by [DeChant and Moradkhani \(2011a; 2011b\)](#), the log-norm
797 perturbation for precipitation is more appropriate. Thus the proposed EFPC approach
798 is further tested through adding 20% log-normal perturbation to the precipitation and
799 20% normal perturbations for the model prediction, streamflow observation, and
800 potential evapotranspiration. Table 8 shows related RMSE, PBIAS, and NSE values.
801 Compared with results in Table 7, adding log-normal perturbation in the precipitation
802 can improve the performance of the proposed method, with the NSE value larger than
803 0.7. Figure 14 presents the comparison between predictions from the hydrologic
804 model and observations as well as PCE results and observations. Figure 15 compares
805 prediction intervals from the hydrologic model and PCE with observations. Both of
806 them show good agreement between model predictions and real observations.

807 -----

808 Place Table 8 and Figures 14 and 15 Here

809 -----

810

811 **5.4. Computational Efficiency of the EFPC Method**

812 The essential ideal of the EFPC approach is to use the ensemble Kalman filter
813 method to estimate the posterior distributions of model parameters and then apply
814 probabilistic collocation method (PCM) to reveal the uncertainty evolution of
815 hydrologic models. Such a method has two advantages in quantifying the uncertainty
816 in hydrologic simulation: (i) the original samples can be drawn from the standard

817 Gaussian distribution, which is easily conducted; (ii) the computational efficiency can
818 be highly improved.

819 The first advantage is straightforward. The second advantage of EFPC will be
820 illustrated through comparing it with traditional Monte Carlo (MC) method. Tables 6
821 and 7 shows the computation efficiency of Monte Carlo method and PCE which are
822 obtained through the proposed EFPC method. In this study, five sample sizes ($n =$
823 500, 1,000, 1,500, 2,000, 2,500) are selected to compare the computation efficiency of
824 MC and the obtained PCE through EFPC. As the sample size increases, the
825 performance of the hydrologic model and PCE would not vary significantly. Both the
826 hydrologic model and PCE produce satisfactory streamflow forecasting in the Xiangxi
827 River. However, the computational efficiency of PCE would be more than ten times
828 faster than the MC method. For example, when $n = 500$, the computational time of
829 MC method would be 54.7 (s), as shown in Table 7, while the computational time of
830 PCE is just 5.3 (s). The ratio of computational efficiency between PCE and MC (time
831 (MC)/time (PCE)) is 10.3. Such a ratio would increase for larger sample sizes (e.g. the
832 ratio is 11.9 for $n = 2,500$). Consequently, the proposed EFPC approach would greatly
833 improve the computational efficiency for uncertainty quantification of hydrologic
834 models

835 In this study, the Hymod was applied to demonstrate the efficiency of the
836 proposed approach. This model is a simple conceptual hydrologic model with five
837 parameters to calibrate. Consequently, the computational requirement for this model is
838 relatively low when compared with other sophisticated models such as semi-
839 distributed and distributed hydrologic models. However, the proposed EFPC approach
840 is more than 10 times faster in computational efficiency for such a simple hydrologic

841 model. The computational efficiency would be improved even more significantly for
842 other complex hydrologic models.

843

844 **5.4. Uncertainty Assessment of Model Parameters**

845 One of the most attraction features for the proposed method is that the
846 polynomial chaos expansion (PCE), with respect to the posterior probabilities of
847 model parameters, can be obtained through the proposed EFPC approach. Such a PCE
848 model can explicitly reveal the contributions of model parameters and their
849 interactions to the total variation in model predictions.

850 In this study, the 5-dimensional 2-order PCE is advanced to reflect the
851 uncertainty propagation of model uncertainty resulting from uncertainty in model
852 parameters. The detailed expression for a 5-dimensional 2-order PCE can be
853 expressed as: $y = a_0 + a_1\zeta_1 + a_2\zeta_2 + a_3\zeta_3 + a_4\zeta_4 + a_5\zeta_5 + a_6(\zeta_1^2 - 1) + a_7(\zeta_2^2 - 1) +$
854 $a_8(\zeta_3^2 - 1) + a_9(\zeta_4^2 - 1) + a_{10}(\zeta_5^2 - 1) + a_{11}\zeta_1\zeta_2 + a_{12}\zeta_1\zeta_3 + a_{13}\zeta_1\zeta_4 + a_{14}\zeta_1\zeta_5 + a_{15}\zeta_2\zeta_3 +$
855 $a_{16}\zeta_2\zeta_4 + a_{17}\zeta_2\zeta_5 + a_{18}\zeta_3\zeta_4 + a_{19}\zeta_3\zeta_5 + a_{20}\zeta_4\zeta_5$, where $\zeta_1, \zeta_2, \zeta_3, \zeta_4, \zeta_5$ are independent
856 standard normal variable representing $C_{max}, b_{exp}, \alpha, R_q$ and R_s , respectively. Since the
857 variables $\zeta_1, \zeta_2, \zeta_3, \zeta_4, \zeta_5$ are standard normal variables, the variance of y can be easily
858 derived, which can be obtained as: $\text{Var}(y) = \text{Var}(a_0 + a_1\zeta_1 + a_2\zeta_2 + a_3\zeta_3 + a_4\zeta_4 + a_5\zeta_5 +$
859 $a_6(\zeta_1^2 - 1) + a_7(\zeta_2^2 - 1) + a_8(\zeta_3^2 - 1) + a_9(\zeta_4^2 - 1) + a_{10}(\zeta_5^2 - 1) + a_{11}\zeta_1\zeta_2 + a_{12}\zeta_1\zeta_3 +$
860 $a_{13}\zeta_1\zeta_4 + a_{14}\zeta_1\zeta_5 + a_{15}\zeta_2\zeta_3 + a_{16}\zeta_2\zeta_4 + a_{17}\zeta_2\zeta_5 + a_{18}\zeta_3\zeta_4 + a_{19}\zeta_3\zeta_5 + a_{20}\zeta_4\zeta_5) = a_1^2 + a_2^2 +$
861 $a_3^2 + a_4^2 + a_5^2 + 2a_6^2 + 2a_7^2 + 2a_8^2 + 2a_9^2 + 2a_{10}^2 + a_{11}^2 + a_{12}^2 + a_{13}^2 + a_{14}^2 + a_{15}^2 +$
862 $a_{16}^2 + a_{17}^2 + a_{18}^2 + a_{19}^2 + a_{20}^2$. Such an expression can explicitly reflect the
863 contribution of the variation in model parameters to the uncertainty of model
864 predictions.

865 Figure 16 shows the comparison of the contributions for different parameters to

866 the total uncertainty in model predictions. The variance ratio is calculated through the
867 coefficients of the obtained PCE and the total variance. For instance the variance ratio
868 of the main effect for C_{max} is generated by $a_1^2 / \text{Var}(y)$. As shown in Figure 16, for the
869 main effect of each parameter, namely $\zeta_1, \zeta_2, \zeta_3, \zeta_4, \zeta_5$, the variable of ζ_5 , indicating the
870 parameter R_q , contributes most to the total variance in model predictions, and also ζ_3
871 and ζ_4 , which respectively represent α and R_s , present apparent contributions to the
872 uncertainty in model outputs. For the quadratic terms, ζ_5^2 would be most sensitive to
873 the uncertainty in model predictions, but other quadratic terms do not show apparent
874 contributions, with all the values less than 0.1 in most simulation periods. Moreover,
875 as shown in Figure 16(c), the interactions among those five parameters only
876 contribute slightly to the variance in model predictions, with the highest variance ratio
877 less than 0.06. Among these interactive effects, the interaction between ζ_3 and ζ_5
878 contributes most to the total variance, followed by the interaction between ζ_3 and ζ_4 .

879 -----
880 Place Figure 16 Here
881 -----

882
883 The proposed EFPC approach can effectively quantify the uncertainty
884 propagation in model simulation resulting from uncertainty model parameters.
885 Particularly, the obtained PCEs are able to express how the uncertainty in model
886 parameters can affect the uncertainty in model predictions, and further identify the
887 main, quadratic and interactive effects of model parameters on the variation in model
888 outputs. Moreover, based on the obtained PCEs, the global sensitivity analysis can be
889 easily conducted without running the original hydrologic model through Monte Carlo
890 method. Such PCE-based global sensitivity analysis has been conducted in our

891 forthcoming paper (Fan et al., 2015b).

892

893 **6. Conclusions**

894 Hydrologic models are designed to simulate the rainfall-runoff processes through
895 conceptualizing and aggregating the complex, spatially distributed and highly
896 interrelated water, energy, and vegetation processes in a watershed into relatively
897 simple mathematical equations. A significant consequence of process
898 conceptualization is that the model parameters exhibit extensive uncertainties, leading
899 to significant uncertainty in hydrologic forecasts. This study proposed an integrated
900 framework for uncertainty quantification of hydrologic models through a coupled
901 ensemble filtering and probabilistic collocation (EFPC) approach. This developed
902 EFPC method combined the backward and forward uncertainty quantification
903 methods together, in which the backward uncertainty quantification method (i.e.
904 EnKF) was employed to reduce model uncertainty and improve the forecast accuracy
905 based on the observed measurements, and the forward method (i.e. PCM) was further
906 used to quantify the inherent uncertainty of the hydrologic model after a data
907 assimilation process.

908 The conceptual hydrologic model, Hymod, was used to demonstrate the
909 applicability of the proposed method in quantifying uncertainties of the hydrologic
910 forecasts. A synthetic experiment was firstly conducted based on a short simulation
911 period (i.e. 365 days). A set of predefined values for model parameters of Hymod
912 were provided to generate streamflows which were considered as the observations in
913 the EnKF adjusting process. After one-year data assimilation process by EnKF, the
914 uncertainty of model parameters (i.e. b_{exp} , α , R_s , R_q) was significantly reduced except
915 the parameter C_{max} . Meanwhile, the uncertainty of the Hymod predictions was also

916 reduced. Afterward, a probabilistic collocation method (PCM) was used to quantify
917 the uncertainty in the Hymod predictions. In PCM, a 4-dimensional 2-order
918 polynomial chaos expansion (PCE) (R_q is considered to be deterministic) was used to
919 approximate the forecasted streamflow, and all potential collocation points were
920 applied to formulate linear regression equations to estimate the unknown coefficients
921 in PCE. The results indicated that the PCE reflected the uncertainty of the streamflow
922 results. The mean and standard deviation values of PCE were consistent with those
923 obtained by Monte Carlo (MC) simulation method, except slight errors existing in the
924 standard deviation values. For the detailed probability density functions, the
925 histograms formulated by the PCE predictions hold similar but slightly steeper shapes
926 to the MC simulation results.

927 The proposed EFPC method was then applied to a real-world watershed in the
928 Three Gorges Reservoir area in China. The impact of relative errors was evaluated for
929 the performance of EnKF for estimating the posterior distributions of hydrologic
930 model parameters. The results showed that 20% of relative error may be appropriate
931 to account for the uncertainties in precipitation, potential evapotranspiration, and
932 streamflow observations in Xiangxi River. The results showed that the polynomial
933 chaos expansion (PCE) is a good representation of the hydrologic model for
934 streamflow forecasting and uncertainty quantification. Specifically, the efficiency of
935 the PCE would be more than 10 times faster than the hydrologic model.

936 This study proposed a coupled ensemble filtering and probabilistic collocation
937 (EFPC) method for quantifying the uncertainty of hydrologic models. The innovation
938 of this study is to integrate EnKF and PCM into a framework, in which the posterior
939 distributions of model parameters are estimated through EnKF, and the uncertainty
940 propagation and evolution from model parameters to hydrologic predictions are

941 characterized by the probabilistic collocation method. Compared with a classic Monte
942 Carlo simulation method, the proposed method can be easily implemented, avoiding
943 drawing samples from arbitrary probability distributions. The computation efficiency
944 can be highly improved by the proposed method.

945

946 **Acknowledgments:** This research was supported by the Natural Science Foundation
947 of China (No. 51190095 and 51225904) and the Program for Innovative Research
948 Team in University (IRT1127).

949

950

951 **References**

- 952 Abaza M., Anctil F., Fortin V., Turcotte R., (2014). Sequential streamflow assimilation for short-
953 term hydrological ensemble forecasting, *Journal of Hydrology*, doi
954 10.1016/j.jhydrol.2014.08.038
- 955 Ajami N.K., Duan Q.Y., Sorooshian S., (2007). An integrated hydrologic Bayesian multimodel
956 combination framework: Confronting input, parameter, and model structural uncertainty in
957 hydrologic prediction. *Water Resources Research*, 43, W01403.
- 958 Assumaning G.A., Chang S.Y., (2014). State and Parameter Estimation in Three-Dimensional
959 Subsurface Contaminant Transport Modeling using Kalman Filter Coupled with Monte Carlo
960 Sampling, *Journal of Environmental Informatics*, 24(2), 80-89.
- 961 Béal D., Brasseur P., Brankart J.-M., Ourmières, Y., Verron J., (2010). Characterization of mixing
962 errors in a coupled physical biogeochemical model of the North Atlantic: Implications for
963 nonlinear estimation using Gaussian anamorphosis. *Ocean Science*, 6, 247-263.
- 964 Beven, K. J., and A. M. Binley (1992). The future of distributed hydrological models: Model
965 calibration and uncertainty prediction. *Hydrologic Processes*, 6, 279–298
- 966 Blanchard E.D., (2010). Polynomial Chaos Approaches to Parameter Estimation and Control
967 Design for Mechanical Systems with Uncertain Parameters. Ph.D Thesis, Department of
968 Mechanical Engineering, Virginia Tech University.
- 969 Chang S.Y., Sayemuzzaman M., (2014). Using Unscented Kalman Filter in Subsurface
970 Contaminant Transport Models. *Journal of Environmental Informatics* 23(1), 14-22
- 971 Clark M.P., Rupp D.E., Woods R.A., Zheng X., Ibbitt R.P., Schmidt A.G., Uddstrom M.J., (2008).
972 Hydrological data assimilation with the ensemble Kalman filter: Use of streamflow
973 observations to update states in a distributed model. *Advances in Water Resources*, 31, 1309-
974 1324.
- 975 Dechant, C., & Moradkhani, H. (2011a). Radiance data assimilation for operational snow and
976 streamflow forecasting. *Advances in Water Resources*, 34(3), 351-364.
- 977 DeChant, C. M., & Moradkhani, H. (2011b). Improving the characterization of initial condition
978 for ensemble streamflow prediction using data assimilation. *Hydrology and Earth System
979 Sciences*, 15(11), 3399-3410.
- 980 DeChant C.M., Moradkhani H., (2012). Examining the effectiveness and robustness of sequential
981 data assimilation methods for quantification of uncertainty in hydrologic forecasting. *Water
982 Resources Research*, 48, W04518, doi:10.1029/2011WR011011
- 983 DeChant C.M., and H. Moradkhani (2014a), Toward a Reliable Prediction of Seasonal Forecast
984 Uncertainty: Addressing Model and Initial Condition Uncertainty with Ensemble Data
985 Assimilation and Sequential Bayesian Combination, *Journal of Hydrology* , 519, 2967-2977,
986 doi: 10.1016/j.jhydrol.2014.05.045.

987 DeChant, C.M. and H. Moradkhani (2014b), *Hydrologic Prediction and Uncertainty*
988 *Quantification*. Handbook of Engineering Hydrology, Modeling, Climate Change and
989 Variability, CRC press, Taylor & Francis Group, PP 387-414.

990 Demaria E.M., Nijssen B., Wagener, T., (2007). Monte Carlo sensitivity analysis of land surface
991 parameters using the Variable Infiltration Capacity model. *Journal of Geophysical Research*,
992 112, D11113.

993 Diks C.G.H., Vrugt J.A., (2010). Comparison of point forecast accuracy of model averaging
994 methods in hydrologic applications. *Stochastic Environmental Research and Risk Assessment*,
995 24, 809-820.

996 Evensen, G. (1994), Sequential data assimilation with a nonlinear quasi-geostrophic model using
997 Monte Carlo methods to forecast error statistics, *Journal Geophysical Research*, 99(C5),
998 10,143–10,162.

999 Fan Y.R., Huang G.H., Huang K., Baetz B.W., (2015a). Planning Water Resources Allocation
1000 under Multiple Uncertainties through A Generalized Fuzzy Two-Stage Stochastic Programming
1001 Method. *IEEE Transactions on Fuzzy Systems*, doi 10.1109/TFUZZ.2014.2362550

1002 Fan Y.R., Huang G.H., Li Y.P., (2012). Robust interval linear programming for environmental
1003 decision making under uncertainty. *Engineering Optimization* 44 (11), 1321-1336

1004 Fan Y.R., Huang G.H., Huang K., Li Y.P., (2015b). Screening Uncertainty and Parameter
1005 Sensitivities of Hydrologic Models through a Hybrid Sequential Data Assimilation and
1006 Probabilistic Collocation Method. Submitted to *Journal of Hydrometeorology*

1007 Fan Y.R., Huang W.W., Huang G.H., Huang K., Zhou X., (2015c). A PCM-based stochastic
1008 hydrological model for uncertainty quantification in watershed systems. *Stochastic*
1009 *Environmental Research and Risk Assessment*, 29, 915-927

1010 Han J.C., Huang G.H., Zhang H., Li Z., Li Y.P., (2014). Bayesian uncertainty analysis in
1011 hydrological modeling associated with watershed subdivision level: a case study of SLURP
1012 model applied to the Xiangxi River watershed, China. *Stochastic Environmental Research and*
1013 *Risk Assessment*. 28(4), 973-989

1014 Herman J.D., Kollat J.B., Reed P.M., Wagener T., (2013). Technical Note: Method of Morris
1015 effectively reduces the computational demands of global sensitivity analysis for distributed
1016 watershed models. *Hydrology and Earth System Sciences*, 17, 2893-2903.

1017 Houska T., Multsch S., Kraft P., Frede H.G., Breuer L., (2014). Monte Carlo-based calibration and
1018 uncertainty analysis of a coupled plant growth and hydrologic model. *Biogeosciences*, 11, 2069-
1019 2082.

1020 Huang S., Mahadevan S., Rebba R., (2007). Collocation-based stochastic finite element analysis
1021 from random field problems. *Probabilistic Engineering Mechanics* 22, 194–205

1022 Johnson R.A., Wichern D.W., (1988). *Applied multivariate statistical analysis*, Prentice Hall
1023 International, NJ, USA

1024 Kalman R.E., (1960). A new approach to linear filtering and prediction problems. *Transactions of*

1025 *the ASME–Journal of Basic Engineering*, 82(1) 35-46.

1026 Kewlani G., Crawford J., Iagnemma K., (2012). A polynomial chaos approach to the analysis of
1027 vehicle dynamics under uncertainty. *Vehicle System Dynamics*, 50, 749-774.

1028 Khu S.T., Werner M.G.F., (2003). Reduction of Monte-Carlo simulation runs for uncertainty
1029 estimation in hydrological modelling. *Hydrology and Earth System Sciences*, 7(5), 680-692

1030 Knighton J., White E., Lennon E., Rajan R., (2014). Development of probability distributions for
1031 urban hydrologic model parameters and a Monte Carlo analysis of model sensitivity, *Hydrologic
1032 Processes*, 28(19), 5131-5139.

1033 Kong X.M., Huang G.H., Fan Y.R., Li Y.P., (2015). Maximum entropy-Gumbel-Hougaard copula
1034 method for simulation of monthly streamflow in Xiangxi river, China. *Stochastic Environmental
1035 Research and Risk Assessment* 29, 833-846.

1036 Leisenring M., Moradkhani H., (2011). Snow water equivalent prediction using Bayesian data
1037 assimilation methods. *Stochastic Environmental Research and Risk Assessment*, 25, 253-270

1038 Leisenring, M., & Moradkhani, H. (2012). Analyzing the uncertainty of suspended sediment load
1039 prediction using sequential data assimilation. *Journal of Hydrology*, 468, 268-282.

1040 Li H., Zhang D., (2007). Probabilistic collocation method for flow in porous media: comparisons
1041 with other stochastic method. *Water Resources Research*, 43.

1042 Li Y., Ryu D., Western A. W., Wang Q. J., (2013). Assimilation of stream discharge for flood
1043 forecasting: The benefits of accounting for routing time lags, *Water Resources Research*, 49,
1044 1887–1900, doi:10.1002/wrcr.20169.

1045 Liu Y., Weerts A.H., Clark M., Hendricks Franssen H.-J., Kumar S., Moradkhani H., Seo D.-J.,
1046 Schwanenberg D., Smith P., van Dijk A.I.J.M., van Velzen N., He M., Lee H., Noh S.J., Rakovec
1047 O., Restrepo P., (2012). Advancing data assimilation in operational hydrologic forecasting:
1048 progresses, challenges, and emerging opportunities. *Hydrology and Earth System Sciences*, 16,
1049 3863-3887.

1050 Lu Z., Zhang D., (2003). On importance sampling Monte Carlo approach to uncertainty analysis for
1051 flow and transport in porous media. *Advances in Water Resources* 26, 1177–1188

1052 Lucas D.D., Prinn R.G., (2005). Parametric sensitivity and uncertainty analysis of dimethylsulfide
1053 oxidation in the clear-sky remote marine boundary layer. *Atmospheric Chemistry Physics*, 5,
1054 1505-1525.

1055 Madadgar, S. and H. Moradkhani (2014). Improved Bayesian Multi-modeling: Integration of
1056 Copulas and Bayesian Model Averaging. *Water Resources Research*, 50, 9586-9603, doi:
1057 10.1002/2014WR015965.

1058 McMillan H.K., Hreinsson E.O., Clark M.P., Singh S.K., Zammit C., Uddstrom M.J., (2013).
1059 Operational Hydrological data assimilation with the recursive ensemble Kalman filter, *Hydrology
1060 and Earth System Science*, 17, 21-38.

1061 Miao D.Y., Huang W.W., Li Y.P., Yang Z.F., (2014). Planning Water Resources Systems under
1062 Uncertainty Using an Interval-Fuzzy De Novo Programming Method, *Journal of Environmental*

1063 Informatics, 24(1), 11-23.

1064 Moore R.J., (1985). The probability-distributed principle and runoff production at point and basin
1065 scales. *Hydrological Sciences Journal*, 30, 273-297

1066 Moore R.J., (2007). The PDM rainfall-runoff model. *Hydrology & Earth System Sciences*, 11(1),
1067 483-499.

1068 Moradkhani, H. (2008). Hydrologic remote sensing and land surface data assimilation. *Sensors*, 8(5),
1069 2986-3004.

1070 Moradkhani, H., S. Sorooshian, H. V. Gupta, and P. Houser (2005a), Dual state – parameter
1071 estimation of hydrologic models using ensemble Kalman filter. *Advances in Water Resources*, 28,
1072 135 – 147.

1073 Moradkhani, H., Hsu, K. L., Gupta, H., & Sorooshian, S. (2005b). Uncertainty assessment of
1074 hydrologic model states and parameters: Sequential data assimilation using the particle filter.
1075 *Water Resources Research*, 41(5)

1076 Moradkhani H., Dechant C.M., Sorooshian S., (2012). Evolution of ensemble data assimilation for
1077 uncertainty quantification using the particle filter-Markov chain Monte Carlo method, *Water*
1078 *Resources Research*, 48, W12520, doi:10.1029/2012WR012144.

1079 Oladyskhin S., Nowak W., (2012). Data-driven uncertainty quantification using the arbitrary
1080 polynomial chaos expansion, *Reliability Engineering and System Safety*, 106, 179-190.

1081 Parrish, M., H. Moradkhani, and C.M. DeChant (2012). Towards Reduction of Model Uncertainty:
1082 Integration of Bayesian Model Averaging and Data Assimilation, *Water Resources Research*, 48,
1083 W03519, doi:10.1029/2011WR011116.

1084 Plaza Guingla D. A., De Keyser R., De Lannoy G. J. M., Giustarini L., Matgen P., and Pauwels V.
1085 R. N., (2013). Improving particle filters in rainfall-runoff models: Application of the resample-
1086 move step and the ensemble Gaussian particle filter, *Water Resource Research*, 49,
1087 doi:10.1002/wrcr.20291.

1088 Reichle R., Mclaughlin D., Entekhabi D., (2002). Hydrologic data assimilation with the ensemble
1089 Kalman filter. *Monthly Weather Review*, 130(1), 103-114.

1090 Schöniger A., Nowak W., Hendricks Franssen H.-J., (2012). Parameter estimation by ensemble
1091 Kalman filters with transformed data: Approach and application to hydraulic tomography. *Water*
1092 *Resources Research*, 48, W04502.

1093 Shi L., Yang J., Zhang D., Li H., (2009). Probabilistic collocation method for unconfined flow in
1094 heterogeneous media. *Journal of Hydrology* 365 4–10

1095 Shi, Y., K. J. Davis, F. Zhang, C. J. Duffy, and X. Yu (2014), Parameter estimation of a physically
1096 based land surface hydrologic model using the ensemble Kalman filter: A synthetic experiment.
1097 *Water Resources Research*, 50, 1-19, doi:10.1002/2013WR014070

1098 Simon E., Bertino L., (2009). Application of the Gaussian anamorphosis to assimilation in a 3-D
1099 coupled physical-ecosystem model of the North Atlantic with the EnKF: A twin experiment.
1100 *Ocean Science*, 5, 495-510

1101 van Delft G., (2007). The Ensemble Particle Filter in Rainfall-Runoff Models. M.S. Thesis, Delft
1102 University of Technology, Delft, Netherlands.

1103 Vrugt J.A., Diks C.G.H., Gupta H.V., Bouten W., Verstraten J.M., (2005). Improved treatment of
1104 uncertainty in hydrologic modelling: Combining the strengths of global optimization and data
1105 assimilation. *Water Resources Research*, 41, W01017.

1106 Vrugt J.A., Sadegh M., (2013). Toward diagnostic model calibration and evaluation: Approximate
1107 Bayesian computation. *Water Resources Research* 49, 4335-4345.

1108 Vrugt J.A., ter Braak C.J.F., Gupta H.V., Robinson B.A., (2009). Equifinality of formal (DREAM)
1109 and informal (GLUE) Bayesian approaches in hydrologic modeling? *Stochastic Environmental*
1110 *Research and Risk Assessment*, 23, 1011-1026.

1111 Wang Dingbao, Chen Yuguo, Cai Ximing, (2009). State and parameter estimation of hydrologic
1112 models using the constrained ensemble Kalman filter. *Water Resources Research*, 45, W11416

1113 Weerts A.H., El Serafy G.Y.H., (2006). Particle filtering and ensemble Kalman filtering for state
1114 updating with hydrological conceptual rainfall-runoff models. *Water Resources Research*, 42,
1115 W09403. doi:10.1029/2005WR004093

1116 Wiener N., (1938). The homogeneous chaos. *American Journal of Mathematics*, 60, 897-936.

1117 Xie X., Zhang D., (2013). A partitioned update scheme for state-parameter estimation of distributed
1118 hydrologic models based on the ensemble Kalman filter. *Water Resources Research*, 49, 7530-
1119 7365

1120 Xiu, D., Karniadakis, G.E., (2002). The Wiener–Askey polynomial chaos for stochastic differential
1121 equations. *SIAM Journal on Scientific Computing* 24, 619–644.

1122 Xiu, D., Karniadakis, G.E., (2003). Modeling uncertainty in flow simulations via generalized
1123 polynomial chaos. *Journal of Computational Physics* 187, 137–167.

1124 Xu H.M., Taylor R.G., Kingston D.G., Jiang T., Thompson J.R., Todd M.C., (2010). Hydrological
1125 modeling of River Xiangxi using SWAT2005: A comparison of model parameterizations using
1126 station and gridded meteorological observations. *Quaternary International*, 226, 54-59

1127 Yang W., Yang Z.F., (2014). Evaluation of Sustainable Environmental Flows Based on the
1128 Valuation of Ecosystem Services: a Case Study for the Baiyangdian Wetland, China. *Journal of*
1129 *Environmental Informatics*, 24(2), 90-100

1130 Yin J., Zhan X., Zheng Y., Hain C.R., Liu J., Fang L., (2015). Optimal ensemble size of ensemble
1131 Kalman filter in sequential soil moisture data assimilation. *Geophysical Research Letters*,
1132 DOI: 10.1002/2015GL063366

1133 Zhang N., Li Y.P., Huang W.W., Liu J., An Inexact Two-Stage Water Quality Management Model
1134 for Supporting Sustainable Development in a Rural System. *Journal of Environmental*
1135 *Informatics*, 24(1), 52-64.

1136 Zhang Y., Li H., Yang D., (2012a). Simultaneous estimation of relative permeability and capillary
1137 pressure using ensemble-based history matching techniques. *Transport in porous media* 94 (1),
1138 259-276.

1139 Zhang Y, Song C, Zheng S, Yang D. (2012b). Simultaneous estimation of relative permeability and
1140 capillary pressure for tight formations from displacement experiments. SPE paper 162663, *the*
1141 *SPE Canadian Unconventional Resources Conference*; 2012 October 30–November 1; Calgary,
1142 AB

1143 Zhang Y., Yang D., (2013). Simultaneous estimation of relative permeability and capillary pressure
1144 for tight formations using ensemble-based history matching method. *Computers & Fluids* 71,
1145 446-460

1146 Zhang Y., Yang D., (2014). Estimation of relative permeability and capillary pressure for tight
1147 formations by assimilating field production data. *Inverse Problems in Science and Engineering*
1148 22 (7), 1150-1175

1149 Zheng Y., Wang W., Han F., Ping J., (2011). Uncertainty assessment for watershed water quality
1150 modeling: A Probabilistic Collocation Method based approach. *Advances in Water Resources* 34
1151 887–898

1152

1153

1154 **List of Figure Captions**

1155 Figure 1. The process of the PCM approach

1156 Figure 2. Description of Hymod

1157 Figure 3. The location of the studied watershed

1158 Figure 4. Comparison between the ensembles of the forecasted and synthetic-
1159 generated true discharge

1160 Figure 5. Convergence of the parameter through the EnKF for the synthetic
1161 experiment over data assimilation period

1162 Figure 6. Histogram of untransformed variable, empirical CDF, histogram of
1163 transformed variable, and normal probability plot for C_{max} (unit (mm)).

1164 Figure 7. The comparison between the mean values of MC simulation and 2-order
1165 PCE results

1166 Figure 8. The comparison between the standard deviation values of MC simulation
1167 and 2-order PCE results

1168 Figure 9. The distribution of the relative errors between the standard deviations from
1169 MC simulation and 2-order PCE prediction results

1170 Figure 10. The comparison between the percentile values of MC simulation and 2-
1171 order PCE results

1172 Figure 11. The comparison of histograms between MC simulation and 2-order PCE
1173 results (note: the left is for MC and the right is for PCE)

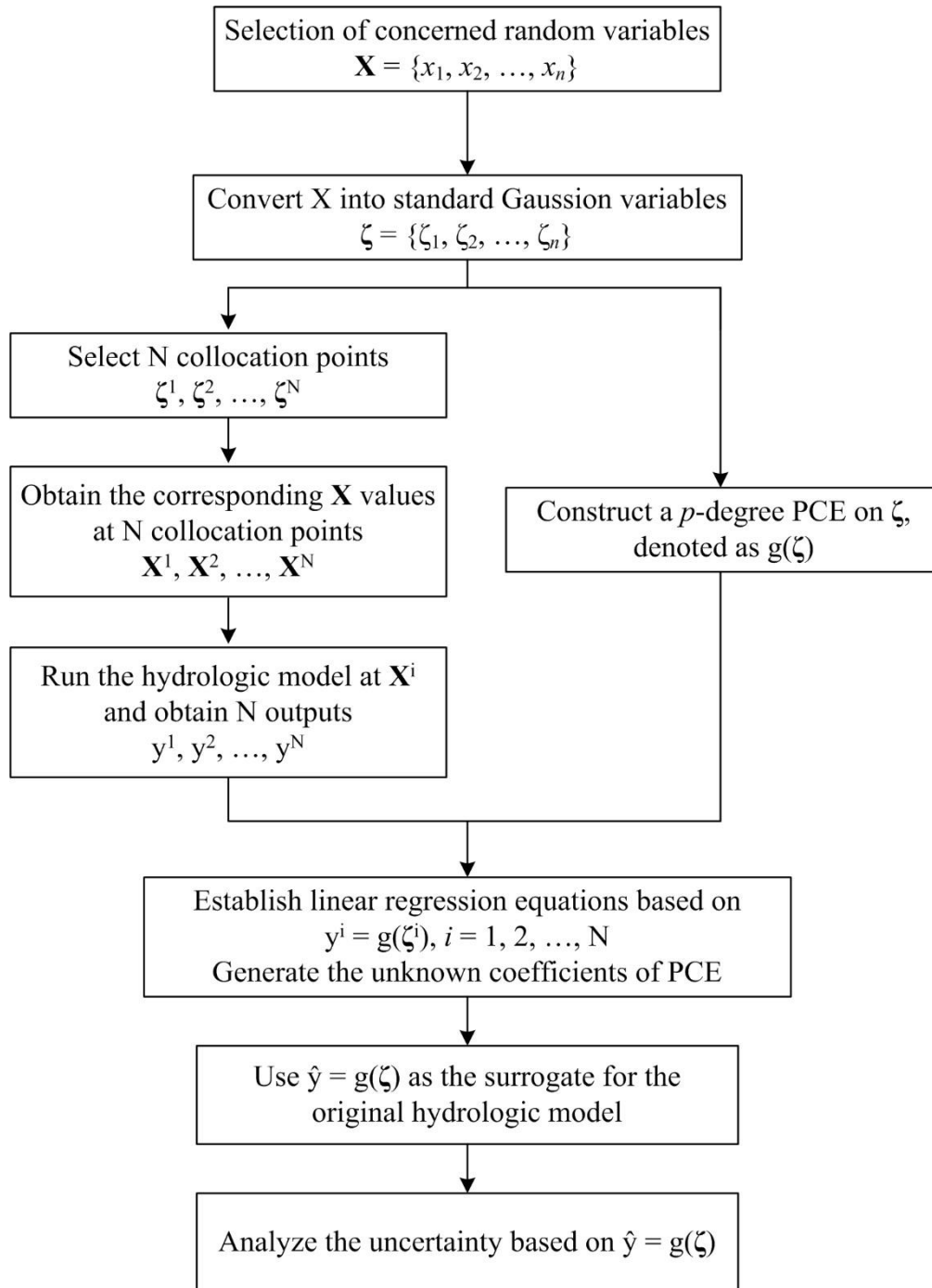
1174 Figure 12 Comparison between the predication means and observations under normal
1175 error assumption for precipitation: (a) hydrologic model predictions vs. observations,
1176 (b) PCE results vs. observation

1177 Figure 13. Comparison between the predication intervals and observations under
1178 normal error assumption for precipitation: (a) hydrologic model prediction intervals
1179 vs. observation, (b) PCE predicting intervals vs. observation

1180 Figure 14. Comparison between the predication means and observations under
1181 lognormal error assumption for precipitation: (a) hydrologic model predictions vs.
1182 observations, (b) PCE results vs. observation

1183 Figure 15. Comparison between the predication intervals and observations under
1184 lognormal error assumption for precipitation: (a) hydrologic model prediction
1185 intervals vs. observation, (b) PCE predicting intervals vs. observation

1186 Figure 16. Contributions of model parameters to the uncertainty in model predictions
1187 over the simulation period

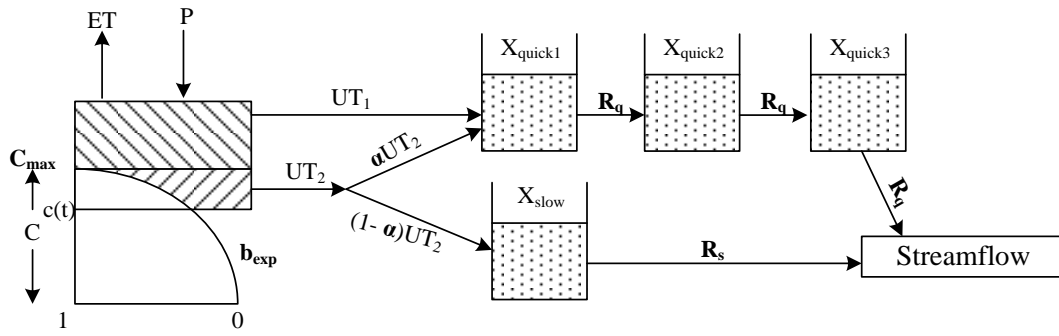


1188

1189

1190

Figure 1. The process of the PCM approach

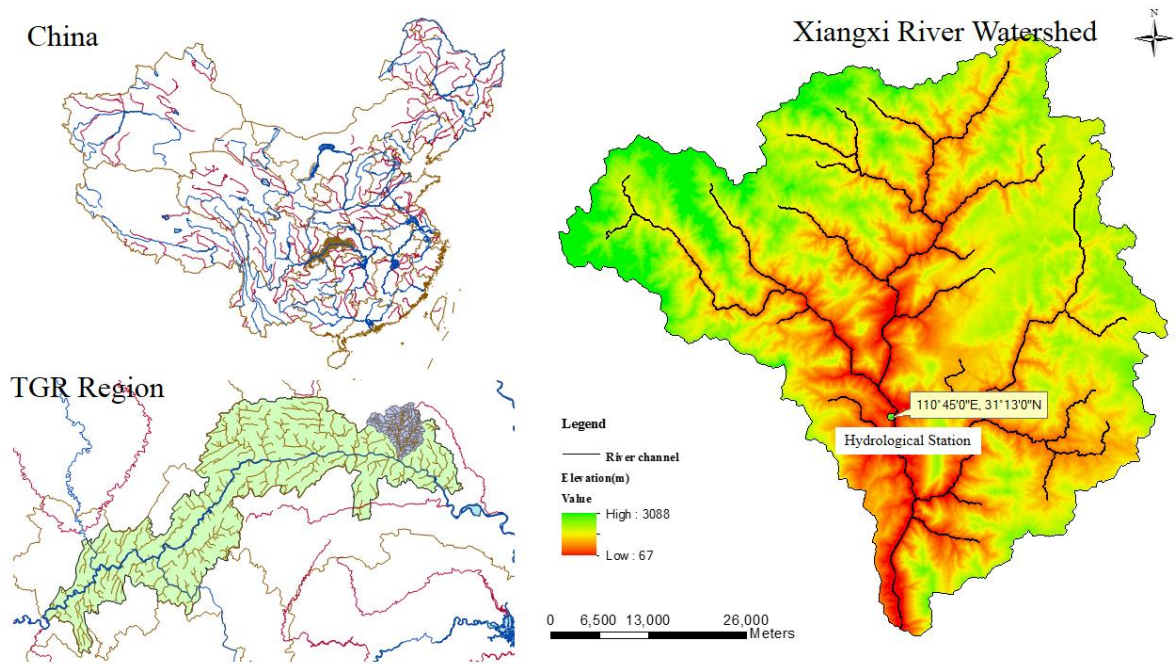


1191

1192

1193

Figure 2 Description of Hymod (modified from Vrugt et al., 2003)

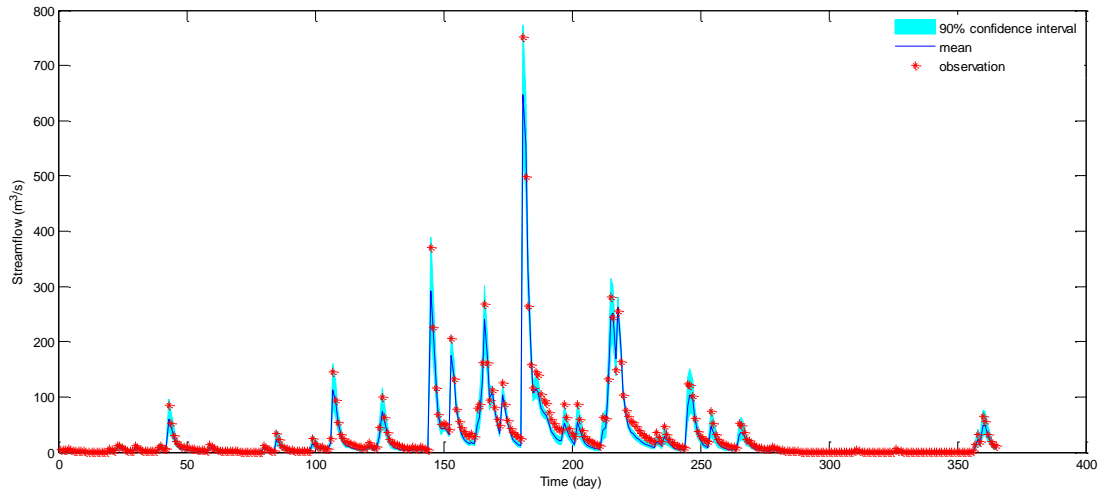


1194

1195

1196

Figure 3: The location of the studied watershed



1197

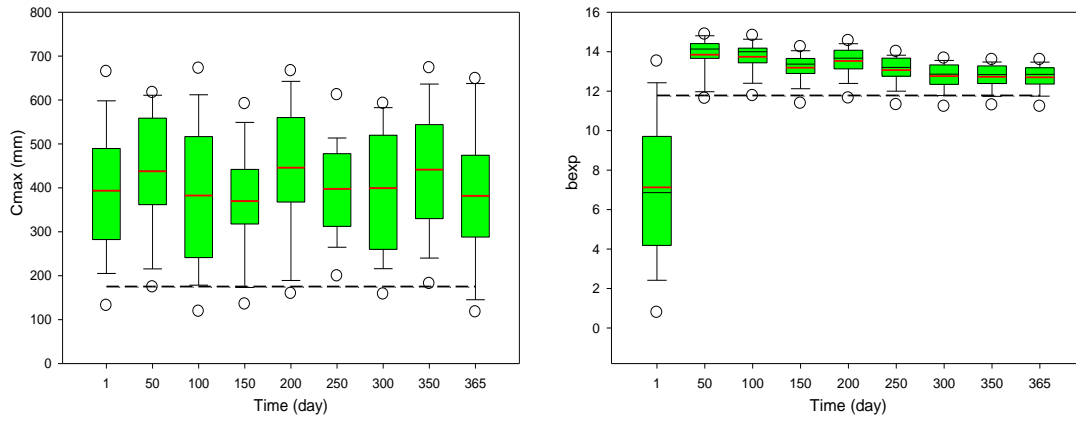
1198

1199

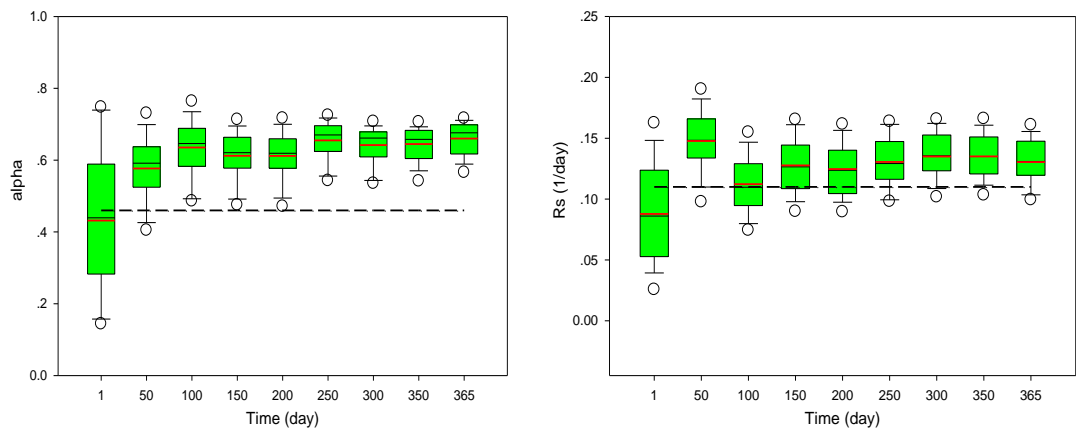
1200

Figure 4. Comparison between the ensembles of the forecasted and synthetic-generated true discharge

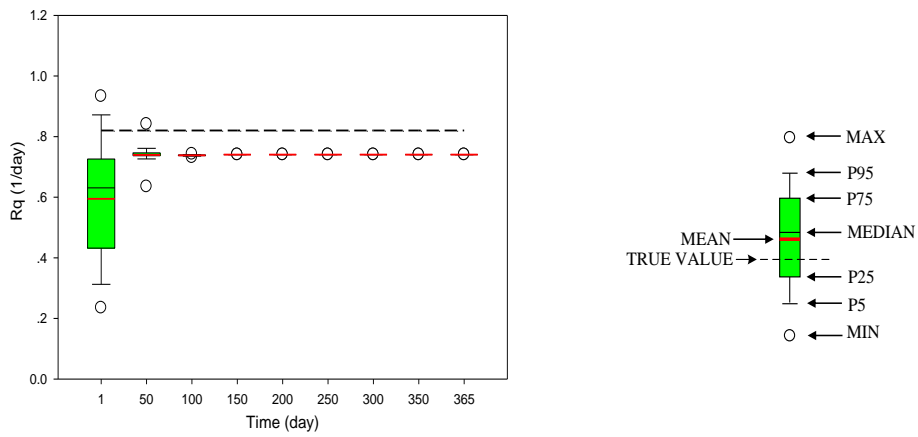
1201



1202



1203



1204

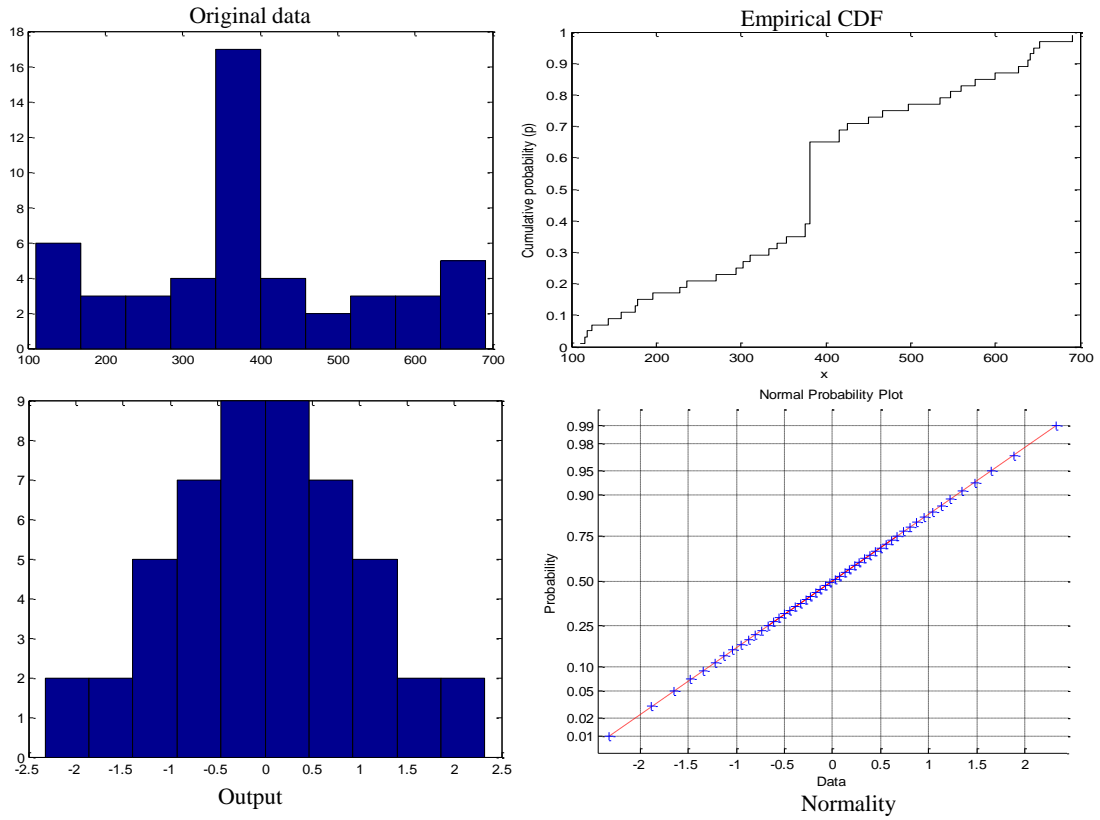
1205

1206

1207

1208

Figure 5. Convergence of the parameter through the EnKF for the synthetic experiment over data assimilation period



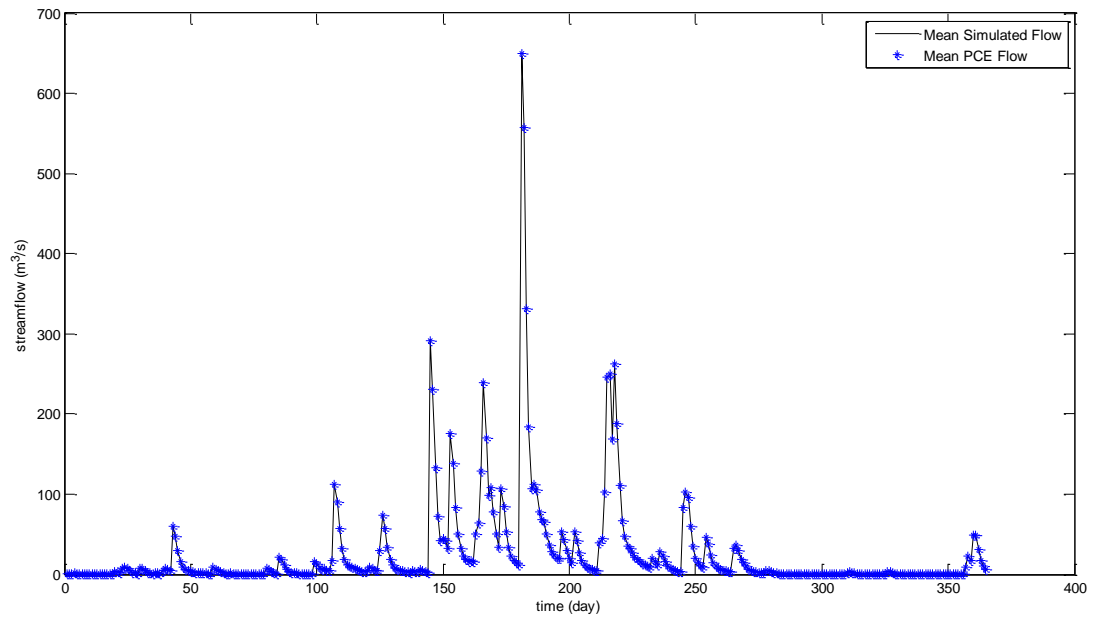
1209

1210

1211

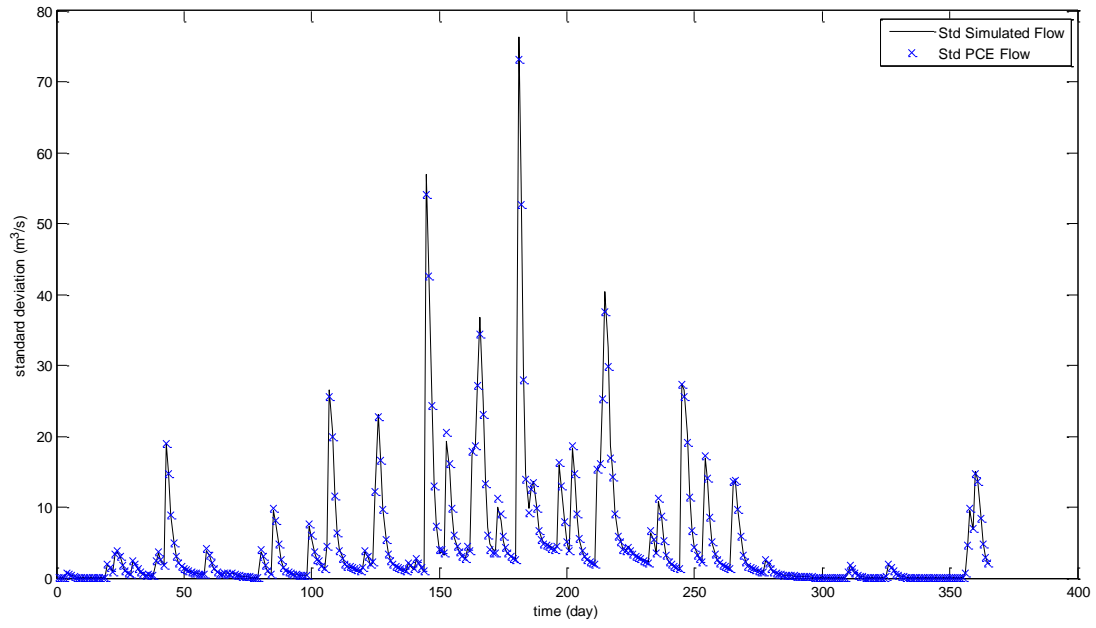
1212

Figure 6. Histogram of untransformed variable, empirical CDF, histogram of transformed variable, and normal probability plot for C_{max} (unit (mm)).



1213
1214
1215
1216
1217
1218

Figure 7. The comparison between the mean values of the MC simulation and 2-order PCE results



1219

1220

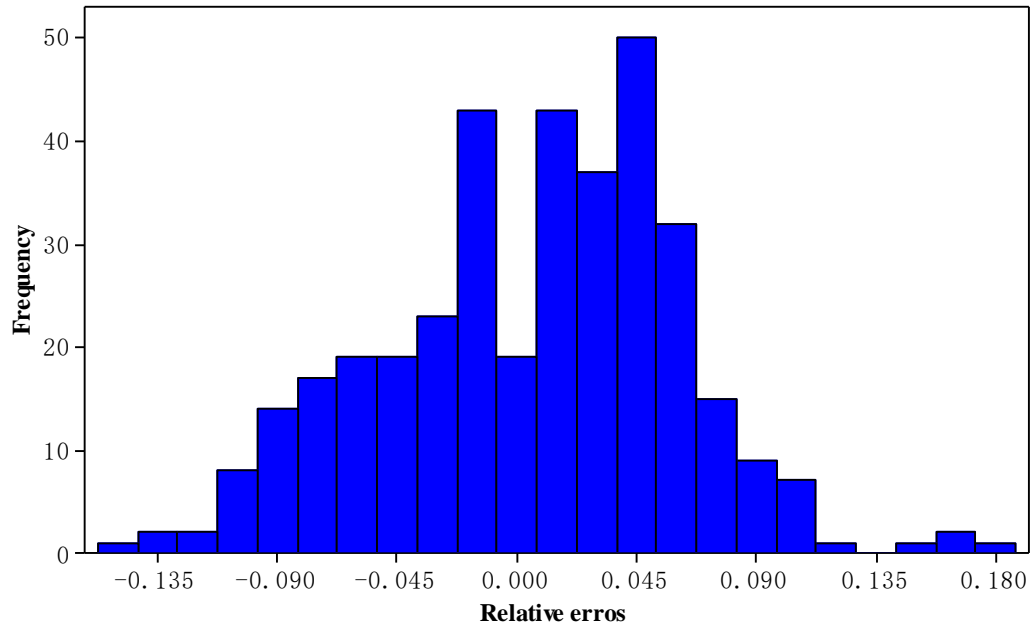
1221

1222

1223

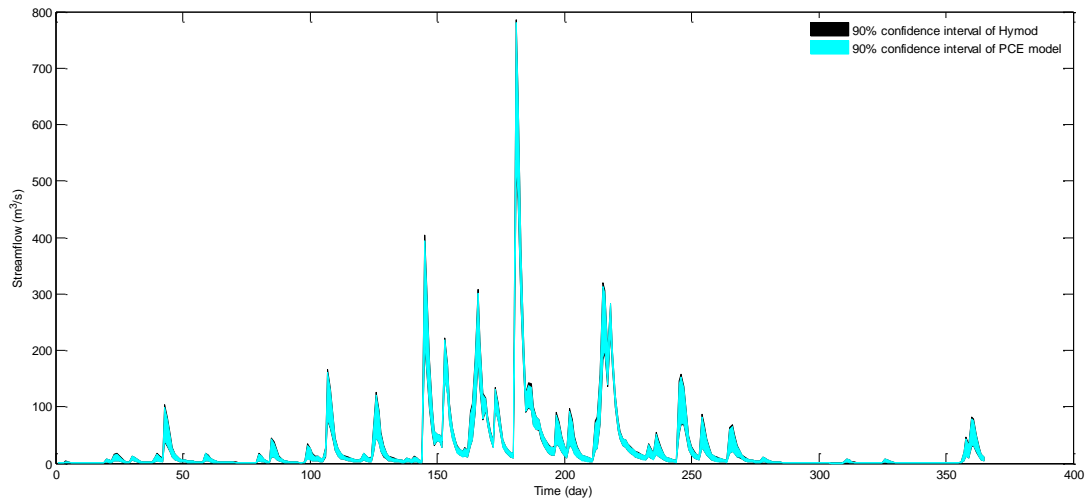
Figure 8. The comparison between the standard deviation values of MC simulation and 2-order PCE results

Histogram of the relative error for standard deviation



1224
1225
1226
1227

Figure 9. The distribution of the relative errors between the standard deviations from MC simulation and 2-order PCE prediction results



1228

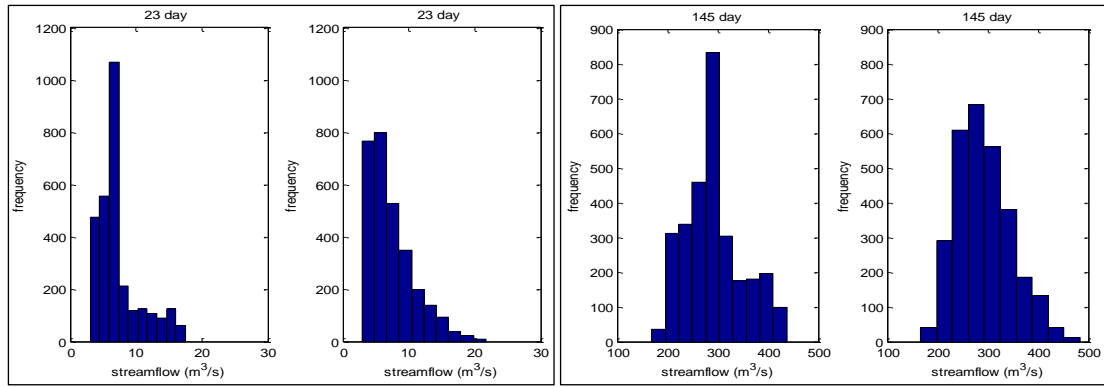
1229

1230

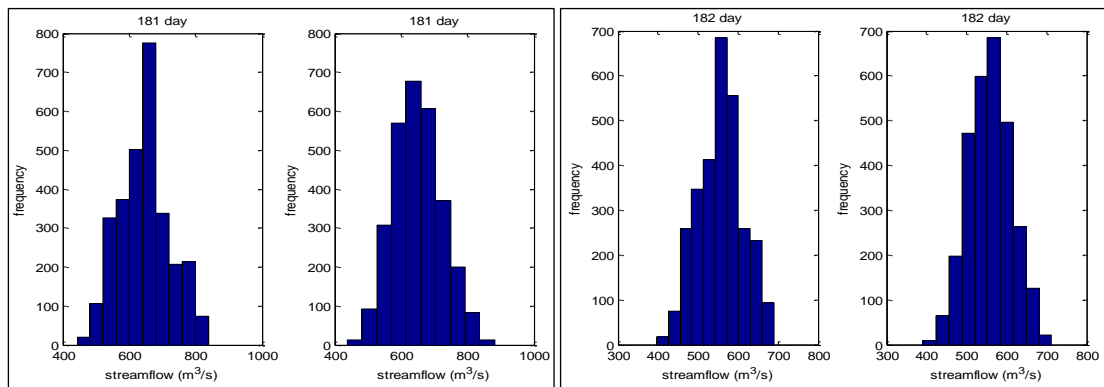
1231

Figure 10. The comparison between the prediction intervals of MC simulation and 2-order PCE results

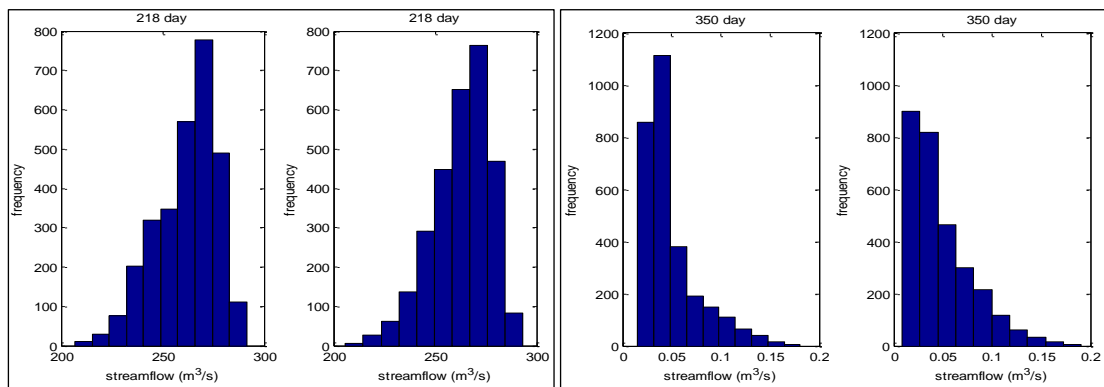
1232



1233



1234



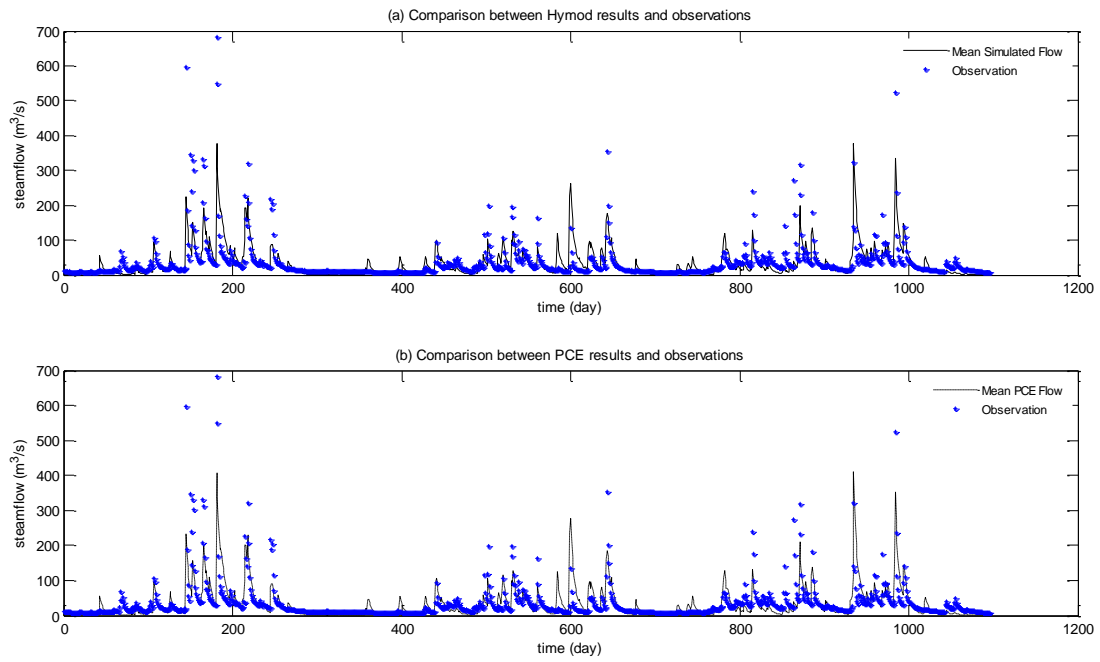
1235

1236

1237

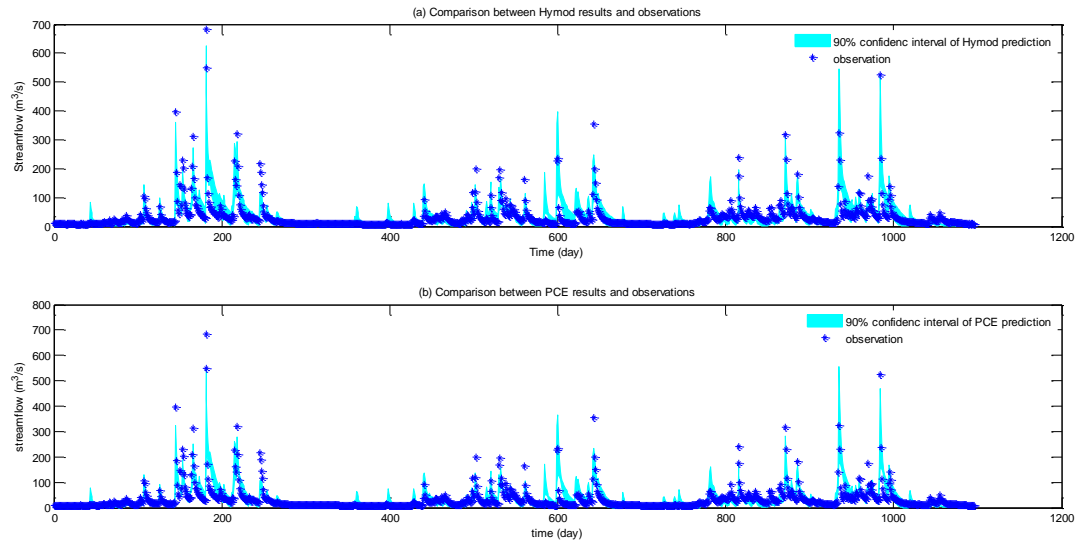
1238

Figure 11. The comparison of histograms between MC simulation and 2-order PCE results (note: in each subfigure, the left column represent MC results and the right one represents the PCE results)



1239
 1240
 1241
 1242
 1243

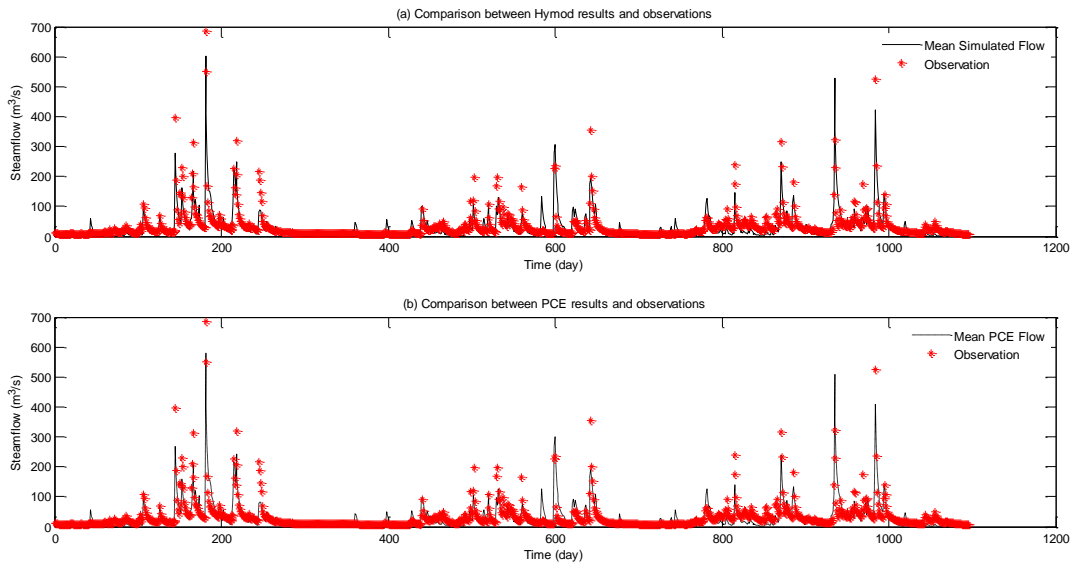
Figure 12. Comparison between the prediction means and observations under normal error assumption for precipitation: (a) hydrologic model predictions vs. observations, (b) PCE results vs. observation



1244

1245 Figure 13. Comparison between the prediction intervals and observations under
 1246 normal error assumption for precipitation: (a) hydrologic model prediction intervals
 1247 vs. observation, (b) PCE predicting intervals vs. observation

1248



1249

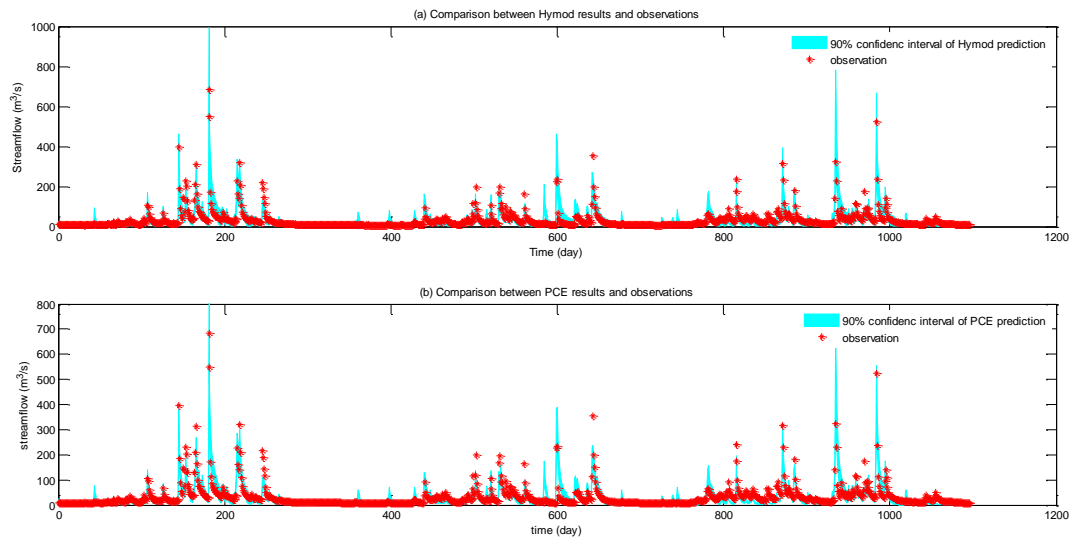
1250 Figure 14. Comparison between the predication means and observations under

1251 lognormal error assumption for precipitation: (a) hydrologic model predictions vs.

1252 observations, (b) PCE results vs. observation

1253

1254



1255
 1256
 1257
 1258
 1259
 1260

Figure 15. Comparison between the prediction intervals and observations under lognormal error assumption for precipitation: (a) hydrologic model prediction intervals vs. observation, (b) PCE predicting intervals vs. observation

1265 **List of Table Captions**

1266 Table 1. Number of the truncated terms for M -dimensional p th order PCE

1267 Table 2. All collocation points for 2-dimensional 2- and 3-ord PCEs

1268 Table 3. The predefined true values and fluctuating ranges for the parameters of Hymod

1269 Table 4. Comparison of the performance of EnKF under different ensemble sizes

1270 Table 5. Comparison of statistic characteristics of the 2-order PCE and MC simulation
1271 results at specific time periods

1272 Table 6 Performance of EnKF under different relative error scenarios

1273 Table 7. Comparison between Monte Carlo method and PCE with normal error
1274 perturbation for precipitation

1275 Table 8. Comparison between Monte Carlo method and PCE with lognormal error
1276 perturbation for precipitation

1277

1278

1279

1280

1281 Table 1. Number of the truncated terms for M -dimensional p th order PCE

	$M = 1$	$M = 2$	$M = 3$	$M = 4$	$M = 5$
$p = 1$	2	3	4	5	6
$p = 2$	3	6	10	15	21
$p = 3$	4	10	20	35	56

1282

1283

1284 Table 2. All collocation points for the 2-dimensional 2- and 3-ord PCEs

Collocation points	Second order		Third order	
	ζ_1	ζ_2	ζ_1	ζ_2
1	-1.73	-1.73	0.00	0.00
2	-1.73	0.00	0.00	-2.33
3	-1.73	1.73	0.00	-0.74
4	0.00	-1.73	0.00	0.74
5	0.00	0.00	0.00	2.33
6	0.00	1.73	-2.33	0.00
7	1.73	-1.73	-2.33	-2.33
8	1.73	0.00	-2.33	-0.74
9	1.73	1.73	-2.33	0.74
10			-2.33	2.33
11			-0.74	0.00
12			-0.74	-2.33
13			-0.74	-0.74
14			-0.74	0.74
15			-0.74	2.33
16			0.74	0.00
17			0.74	-2.33
18			0.74	-0.74
19			0.74	0.74
20			0.74	2.33
21			2.33	0.00
22			2.33	-2.33
23			2.33	-0.74
24			2.33	0.74
25			2.33	2.33

1285

1286

1287

1288

1289

Table 3. The predefined true values and fluctuating ranges for the parameters of Hymod

	Parameters				
	C_{max} (mm)	b_{exp}	α	R_s (1/day)	R_q (1/day)
True	175.40	11.68	0.46	0.11	0.82
Primary range	[100, 700]	[0.10, 15]	[0.10, 0.80]	[0.001, 0.20]	[0.10, 0.99]
EnKF results	[110.9, 690.6]	[10.2, 13.8]	[0.56, 0.73]	[0.10, 0.16]	[0.75, 0.76]

1290

1291

1292 Table 4. Comparison of the performance of EnKF under different ensemble sizes

Ensemble Size	30	50	100	150	200	300
NSE	0.771	0.731	0.727	0.672	0.652	0.738
PBIAS	8.917	10.172	10.424	13.023	10.429	12.029
RMSE	32.186	34.880	35.236	38.415	39.480	49.831

1293

1294

1295 Table 5. Comparison of statistic characteristics of the 2-order PCE and MC
 1296 simulation results at specific time periods

Time (d)	Mean		Standard Deviation		Kurtosis		Skewness	
	PCE	MC	PCE	MC	PCE	MC	PCE	MC
23	7.38	7.35	3.35	3.22	4.30	4.07	1.27	1.38
145	292.05	292.17	54.04	56.88	2.93	2.63	0.56	0.48
181	649.71	647.20	73.11	76.28	2.70	2.56	0.20	0.13
182	558.05	555.92	52.64	55.47	2.67	2.53	0.02	-0.04
218	263.00	261.77	14.19	15.00	3.27	2.98	-0.68	-0.70
350	0.05	0.05	0.03	0.03	4.64	5.59	1.35	1.67

1297

1298

1299 Table 6 Performance of EnKF under different relative error scenarios

1300

Relative error	10%	15%	20%	25%	30%
RMSE	42.4	43.8	37.1	37.4	39.2
PBIAS(%)	27.4	22.5	6.0	13.8	13.6
NSE	0.63	0.64	0.65	0.64	0.64

1301

1302

1303

1304 Table 7 Comparison between hydrologic model and PCE with normal error perturbation for
 1305 precipitation

Sample size		500	1000	1500	2000	2500
Hydrologic Model	RMSE	37.118	37.134	37.107	37.099	37.101
	PBIAS(%)	6.043	6.124	6.053	5.755	5.857
	NSE	0.6475	0.6473	0.6476	0.6478	0.6468
	Time (s)	54.697	111.478	166.210	232.847	334.471
PCE	RMSE	37.394	37.349	37.360	37.310	37.339
	PBIAS(%)	7.062	7.444	7.257	7.222	7.238
	NSE	0.6441	0.6417	0.6433	0.6429	0.6423
	Time (s)	5.278	8.750	14.044	19.050	28.232

1306

1307

1308

1309 Table 8. Comparison between hydrologic model and PCE with lognormal error perturbation for
 1310 precipitation

Sample size		500	1000	1500	2000	2500
Hydrologic Model	RMSE	27.1144	27.1248	27.1438	27.1004	27.1379
	PBIAS(%)	18.7209	18.5018	18.4552	18.5887	18.4069
	NSE	0.7185	0.7182	0.7178	0.7187	0.7179
	Time (s)	56.8370	107.4660	173.3930	240.7350	305.1020
PCE	RMSE	27.3754	27.4964	27.4632	27.3709	27.4515
	PBIAS(%)	18.6222	18.5811	18.5557	18.6772	18.6420
	NSE	0.7130	0.7105	0.7111	0.7131	0.7114
	Time (s)	5.7430	9.1590	16.3160	19.0140	22.1320

1311

1312